

Copyright  
by  
Erick Leuro  
2014

The Dissertation Committee for Erick Leuro  
certifies that this is the approved version of the following dissertation:

**Spatial and Temporal Distributions of Accumulation Rates on  
the Catchment of Thwaites Glacier, West Antarctica**

Committee:

---

Don Blankenship, Supervisor

---

Clark Wilson

---

John Holt

---

Liang Yang

---

Mrinal Sen

**Spatial and Temporal Distributions of Accumulation Rates on  
the Catchment of Thwaites Glacier, West Antarctica**

**by**

**Erick Leuro, B.S., M.S Geo. Sci.**

**DISSERTATION**

Presented to the Faculty of the Graduate School of  
The University of Texas at Austin  
in Partial Fulfillment  
of the Requirements  
for the Degree of

**DOCTOR OF PHILOSOPHY**

THE UNIVERSITY OF TEXAS AT AUSTIN

May 2014

Dedicated to my parents.

## Acknowledgments

I wish to thank my advisor Don Blankenship for his unconditional support, advice, encouragement in every aspect of my academic life: academic, professional, and as an individual, Don. I want you to know that I don't overlook that as a professor you have gone the extra mile to support me, a million thanks for it.

Many thanks to my committee for all their support, their teaching and for helping me visualize the standards that I must pursue as an earth scientist.

I want to especially thank Duncan Young for his collaboration during all the stages of this work by sharing his knowledge, skills, expertise and uncanny good memory. Duncan, a millions thanks to you for all the long hours working with me and also for our science discussions. You really have helped me to look at Antarctica in a more critical, broad and in-depth manner.

Thanks to all the members of the cryosphere team, specially to Gail, Enrica, Arami, Evelyn, Aly, Marie, all your help in the last stages of the thesis was really invaluable. Thanks to Jamin, you really know how to encourage people! I also want to mention Sasha, Hunter, Irina, Theresa, and Dusty for all the valuable science conversations. They really helped me to grow my understanding of the continent. They were invaluable to me.

Thank you to all my good friends in Austin that have made a positive impact on me: Nacho, Miguel, Gonzo, David, Alan, Wilbert, Rafa, Esti, Christine, Tricia,

Kevin, Armando, and all others I am not mentioning here.

Thanks to my friends in Houston and my employer ION-GXT for the continuing support.

Thanks to all my good friends back in Colombia.

Finally, thanks to all my family for their encouragement all this time, especially my nephews and nieces: Paula, Melanie, Rommel, Brandon, Dereck, Valeria and Stephen.

# **Spatial and Temporal Distributions of Accumulation Rates on the Catchment of Thwaites Glacier, West Antarctica**

Publication No. \_\_\_\_\_

Erick Leuro, Ph.D.

The University of Texas at Austin, 2014

Supervisor: Don Blankenship

We make a first-order calculation of accumulation rates in the catchment of Thwaites Glacier (TG), West Antarctica using the Nye and Daansgard-Johnson methodologies. Both formulations compute accumulations as a function of the age-depth relationship, including a thinning correction due to ice flow. For this purpose, I track and firn-correct two continuous, shallow ice layers obtained from radio echo soundings surveyed during the 2004-05 AGASEA expedition. The layers range from 60 to 700 meters depth between the ice divide and the coast. Dating of layers come from the ice core WDC06A, located on the West Antarctic Ice Sheet (WAIS) ice divide, which have ages 548 and 725 years, respectively. We compare our accumulation results with four independent datasets: 1) IceBridge snow radar (2009-2010), optimized for tracking near-surface layers; 2) a contemporary model of snowfall precipitation, 3) an interpolation of ice core data using satellite passive microwave; 4) ice cores data. We test the hypothesis that accumulation rates have

increased since the beginning of the industrial era, a change that has not been observed. Indeed, I find that observations indicate that accumulation rates in the TG catchment have not changed during the past  $\sim 700$  years. From here I assess the mass balance of the system and analyze what it tells about the history of the glacier.



# Table of Contents

<b>Acknowledgments</b>	<b>v</b>
<b>Abstract</b>	<b>vii</b>
<b>List of Tables</b>	<b>xi</b>
<b>List of Figures</b>	<b>xii</b>
<b>Chapter 1. Introduction</b>	<b>1</b>
<b>Chapter 2. Area Description</b>	<b>3</b>
2.1 The Antarctic continent . . . . .	3
2.2 West Antarctica . . . . .	4
2.2.1 Geography . . . . .	4
2.2.2 Geological Setting . . . . .	6
2.2.3 Surface and subglacial topography . . . . .	7
2.2.4 Climate . . . . .	9
2.3 Thwaites Glacier . . . . .	11
2.4 Data Acquisition for this Work . . . . .	13
2.5 Radar Data Set . . . . .	14
<b>Chapter 3. Millennial scale accumulation rates over the catchment of             Thwaites Glacier, Antarctica</b>	<b>16</b>
3.1 Introduction . . . . .	16
3.2 Radar Data . . . . .	17
3.3 Ice Core Chronologies . . . . .	19
3.4 Firn Correction . . . . .	21
3.5 Age of Layers . . . . .	21
3.6 Models . . . . .	23

3.6.1	Nye Model . . . . .	23
3.6.2	Dansgaard-Johnsen Model . . . . .	24
3.7	Results . . . . .	25
3.8	Comparison of Long Term and Modern Accumulation Rates . . . . .	30
3.8.1	RACMO2.1 and AMSR Derived Accumulation Estimates . . . . .	32
3.8.2	Ice Cores ITASE 01-1 and WDC06A . . . . .	34
3.8.3	Accumulation as a Function of Elevation . . . . .	36
3.9	Discussion . . . . .	38
3.10	Conclusions . . . . .	40
 <b>Chapter 4. Paleoaccumulation rates over the fast flow area of Thwaites Glacier using a flux based method</b>		<b>42</b>
4.1	Introduction . . . . .	42
4.2	Methodology . . . . .	43
4.3	Computation Of Flow Lines . . . . .	48
4.4	Sources Of Error . . . . .	49
4.5	Interpretation of Results . . . . .	51
4.6	Comparison with RACMO2.1 and AMSR Inferences of Accumulation	54
4.7	Conclusions . . . . .	58
 <b>Chapter 5. Long Term Mass Balance Of Thwaites Glacier, West Antarctica</b>		<b>60</b>
5.1	Introduction . . . . .	60
5.2	Area Description . . . . .	61
5.3	Data . . . . .	61
5.4	Mass Balance Estimations . . . . .	62
5.5	Ice Volume Retained . . . . .	63
5.5.1	Sources of error in ice volume retained . . . . .	65
5.6	Ice Volume Lost . . . . .	67
5.7	Discussion of Results . . . . .	69
5.8	Conclusions . . . . .	70
 <b>Chapter 6. Summary/Conclusions</b>		<b>72</b>
 <b>Vita</b>		<b>92</b>

## List of Tables

3.1	Ice Cores, Mean Accumulation Values at WAIS, i.e., $\text{myr}^{-1}$ . . . . .	20
3.2	Accumulations Values at WDCO6A and ITASE-01-1 . . . . .	36
5.1	Input Mass for TG, adapted from Medley et al. [2013] $\text{Gtyr}^{-1}$ . . . . .	63
5.2	Ice lost over the grounding line ( $\text{km}^3$ ) and implied total input fluxes ( $\text{km}^3\text{yr}^{-1}$ ) . . . . .	69
5.3	Mass Balance of TG ( $\text{Gtyr}^{-1}$ ), adapted from Medley et al. [2014] and Mougnot et al. [2014] . . . . .	70

## List of Figures

2.1	Ice flow in Antarctica from Rignot et al. [2011]. West Antarctica is on the left hand side of the figure. . . . .	5
2.2	Context figure for Thwaites Glacier, from Holt et al. [2006]. a) bed elevation context in West Antarctic [Lythe et al., 2001], b) AGASEA derived bed elevations, c) Surface and bed elevations along the yellow transect in b, d) datasets in this compilation. The dataset used for this thesis in in orange, e) 1996 ice flow velocities from InSAR [Rignot et al., 2003], f) Ice thickness, 3 km contour shown, g) deglaciaded topography. . . . .	12
3.1	Patterns of ice equivalent accumulation in TG: a) location map with balance velocities after Le Brocq et al. [2006]; b) and c) interpreted layer depths (ice equivalent); d) and e) accumulations rates using Nye [1963]; f) accumulation rates using Dansgaard and Johnsen [1969] for lay2; g) remote sensing derived interpolation [Arthern et al., 2006]; h) the RACMO2.1 atmospheric model of precipitation [Lenaerts et al., 2012b]; d) filtered version of e) with ice core locations. In all panels: black contours, surface elevations [Fretwell et al., 2013]; red line, threshold where $D$ [Waddington et al., 2007] equals 0.5; white line; TG catchment [Vaughan et al., 2001]. Figures 3.2 to 3.8 are expanded versions of these maps. . . . .	18
3.2	Ice equivalent depth for layer 1. Black contours, surface elevations [Fretwell et al., 2013]; red line, threshold where $D$ [Waddington et al., 2007] equals 0.5; white line; TG catchment [Vaughan et al., 2001]. . . . .	26
3.3	Ice equivalent depth for layer 2. Black contours, surface elevations [Fretwell et al., 2013]; red line, threshold where $D$ [Waddington et al., 2007] equals 0.5; white line; TG catchment [Vaughan et al., 2001]. . . . .	27
3.4	Nye inferred ice accumulation rates for layer 1. Black contours, surface elevations [Fretwell et al., 2013]; red line, threshold where $D$ [Waddington et al., 2007] equals 0.5; white line; TG catchment [Vaughan et al., 2001]. . . . .	28
3.5	Nye inferred ice accumulation rates for layer 2. Black contours, surface elevations [Fretwell et al., 2013]; red line, threshold where $D$ [Waddington et al., 2007] equals 0.5; white line; TG catchment [Vaughan et al., 2001]. . . . .	29

3.6	Dansgaard-Johnsen inferred ice accumulation rates for layer 2, using a $h'$ of 0.2. Black contours, surface elevations [Fretwell et al., 2013]; red line, threshold where $D$ [Waddington et al., 2007] equals 0.5; white line; TG catchment [Vaughan et al., 2001]. . . . .	30
3.7	Filtered Nye accumulation for layer 2, over 30 km for comparison with models of accumulation. Black contours, surface elevations [Fretwell et al., 2013]; red line, threshold where $D$ [Waddington et al., 2007] equals 0.5; white line; TG catchment [Vaughan et al., 2001]. . . . .	31
3.8	AMSR interpolation of surface measurements [Arthern et al., 2006]. Black contours, surface elevations [Fretwell et al., 2013]; red line, threshold where $D$ [Waddington et al., 2007] equals 0.5; white line; TG catchment [Vaughan et al., 2001]. . . . .	32
3.9	RACMO 2.1 ice accumulation rates [Lenaerts et al., 2012b]. Black contours, surface elevations [Fretwell et al., 2013]; red line, threshold where $D$ [Waddington et al., 2007] equals 0.5; white line; TG catchment [Vaughan et al., 2001]. . . . .	33
3.10	Radargram along a flowline showing mayor features like surface, bedrock topography, englacial layers. Ice divide its a the left, and grounding line at the right. Notice the lack of ilumination at the grouding layer produced by heavy creavassing. Box indicates shallow layers . . . . .	34
3.11	Radargram zoom. Arrows indicate layers used for this work. Upper layer is called layer 1, and deeper layer is called layer 2 . . . . .	35
3.12	Accumulation rates averaged over 50 m elevation bins, integrated over the entire catchment. Given the sparser coverage in Medley et al. [2013], we do not directly compare those results to ours, but instead add their deviation between RACMO2 and the snow radar result to the full catchment RACMO numbers. . . . .	37
4.1	InSAR surface velocities [Rignot et al., 2011] . . . . .	44
4.2	Coordinate axis along a flow line [Reeh, 1988], Figure 1a. . . . .	46
4.3	Comparison between our flow lines (red lines) and layer flow lines picks identified in englacial structures (green dots) and confirmed by modern GPS [Conway et al., 2010], both showing approximate agreement. . . . .	50
4.4	Blending of accumulations rates from Nye and Reeh for Layer 1. Mount Takahe is at -1400E, -580N . . . . .	52
4.5	Blending of accumulations rates from Nye and Reeh for Layer 2. Mount Takahe is at -1400E, -580N . . . . .	53

4.6	Comparison of different accumulation rates models as a function of elevation, including the InSAR velocity reduced to 75% that matches RACMO. AMSR is the Arthern et al. [2006] interpolation. Red vertical line represents $D=1$ . . . . .	56
4.7	The RACMO2.1 atmospheric model of surface mass balance [Lenaerts and van den Broeke, 2012] . . . . .	57
5.1	Map of the depth to layer 1, using the Thwaites Glacier catchment and lack of data as a mask. The background is the Mosaic of Antarctica (MOA) [Scambos et al., 2007] . . . . .	64
5.2	Map of the depth to layer 2, using the Thwaites Glacier catchment and lack of data as a mask. The background is the Mosaic of Antarctica (MOA) [Scambos et al., 2007] . . . . .	65
5.3	Diagram of the concepts of the total ice volume deposited, retained and lost. . . . .	68

# **Chapter 1**

## **Introduction**

I propose to assess the distribution of accumulation rates in the catchment of Thwaites Glacier (TG) averaged over the last 700 years to determine if they have deviated from the contemporary distribution of accumulation rate from climate modeling. For comparison, I will assess the accumulation rate for the thousand years of natural change prior to the modern industrial world. I will use airborne ice penetrating radar data collected by UTIG in 2004/2005 [Holt et al., 2006], estimated horizontal ice velocities, [Rignot et al., 2011] and layer age dates from ice cores [Sowers, 2010]. Previous work on the mass balance of the West Antarctic Ice Sheet (WAIS) include those of Spikes et al. [2003] in the center of West Antarctica, and Rignot and Thomas [2002] for the TG tongue. In addition, a compilation of Antarctic mass balance by Vaughan et al. [1999] shows the accumulation rates in the WAIS are higher than in East Antarctica but lower than in the Antarctica Peninsula. Within the WAIS, the catchments of TG and Pine Island Glacier (PIG) present higher accumulations than those farther south. As a general trend in the whole continent, the higher values of accumulation are distributed along the coast where accumulation rates are driven by katabatic winds and proximity to the ocean [Lenaerts et al., 2012a].

As explained in the subsequent sections, the accumulation rates will be calculated using two approaches that complement each other; first, temporal and spatial distributions of accumulation rates will be calculated in areas close to the ice divide, where the horizontal velocity is comparatively low. This approach uses my interpreted shallow layer geometry and relies on a simple relation that calculates the accumulation rate as a function of the ice thickness given a known time of deposition for marked layers at a few sites, plus a correction for vertical compaction [Nye, 1963].

In the second approach, the accumulation rates will be calculated using an inverse method from orbital InSAR-derived surface velocities, [Rignot et al., 2011] along flow lines, where shear deformation is assumed to be small, using thicknesses of the interpreted radar layers. In this approach there are areas where the surface velocity is too small for orbital measurements, so the accumulation rates calculated from the first method will be extrapolated to these places. Sources of noise in the accumulation must be identified and removed. These include vertical strain rate, from the divergence/convergence of ice flow associated with areas of steep topography and firn compaction which is a near surface process of transformation from snow to ice.



## **Chapter 2**

### **Area Description**

#### **2.1 The Antarctic continent**

Generally speaking, Antarctica is the southernmost, coldest, driest and windiest continent on the planet. It is covered almost entirely by ice, approximately 98%, with an average thickness of 1.6 km giving to Antarctica the highest average elevation of all the continents. As the largest reservoir of fresh water in the world in the form of ice, Antarctica presents complex interactions with the oceans, the climate, the subglacial topography and the upper crust in a wide range of spatial and temporal scales that go from local to global and from the minute to the geological period [Bindschadler, 2006a]. Among the plethora of geophysical phenomena observed in Antarctica, mass balance is a critical process that influences and is influenced by all of the above mentioned components of the Antarctic system; it is defined as the difference of mass input (snow fall or accumulation rates) and mass output (calving of glaciers and surface melting to a lesser extent).

Mass balance determines the amount of sea level change, the extent of sea ice, and the surface velocity of ice streams and ice sheets, directly influences the magnitude and rate of the isostatic rebound, is also an indicative factor of the amount of surface temperature and moisture content in the Antarctic atmosphere

and determines the state of health of a glacier (i.e. steady or unsteady ice flow). Changes in mass balance could also influence the potential collapse of ice sheets in sectors of the continent, such as West Antarctica, as a response of a combination of internal and external forcing that is large enough to raise the sea level by 5 meters [Rignot et al., 2004]. All of these interactions are the object of vigorous research by the scientific community, as briefly outlined in the next sections, along with the description of the related geological features and processes for the area of West Antarctica, particularly the sector dominated by Thwaites Glacier.

## **2.2 West Antarctica**

### **2.2.1 Geography**

In the context of mass balance and following the presentation by Bindshadler [Bindshadler, 2006a], Antarctica is divided into three main sectors: East Antarctica, West Antarctica and the Antarctica Peninsula. They have areas of  $10.35 \times 10^6 \text{ km}^2$ ,  $1.97 \times 10^6 \text{ km}^2$  and  $0.52 \times 10^6 \text{ km}^2$ , respectively. These values add up to an area comparable to the United States and each one has corresponding ice coverage of 98%, 97% and 80%, respectively. East and West Antarctica are separated by the Transantarctic Mountains, a 3500 km long mountain system that runs across the Antarctic continent and contains the Antarctica Peninsula which extends 950 km from West Antarctica to near Patagonia in South America. The other limits of the West Antarctic Ice Sheet (WAIS), besides the Transantarctic Mountains, are the Weddell, Bellinghousen, Amundsen and Ross Sea Embayments. They are drained mainly by the two largest ice glaciers in West Antarctica: Thwaites Glacier

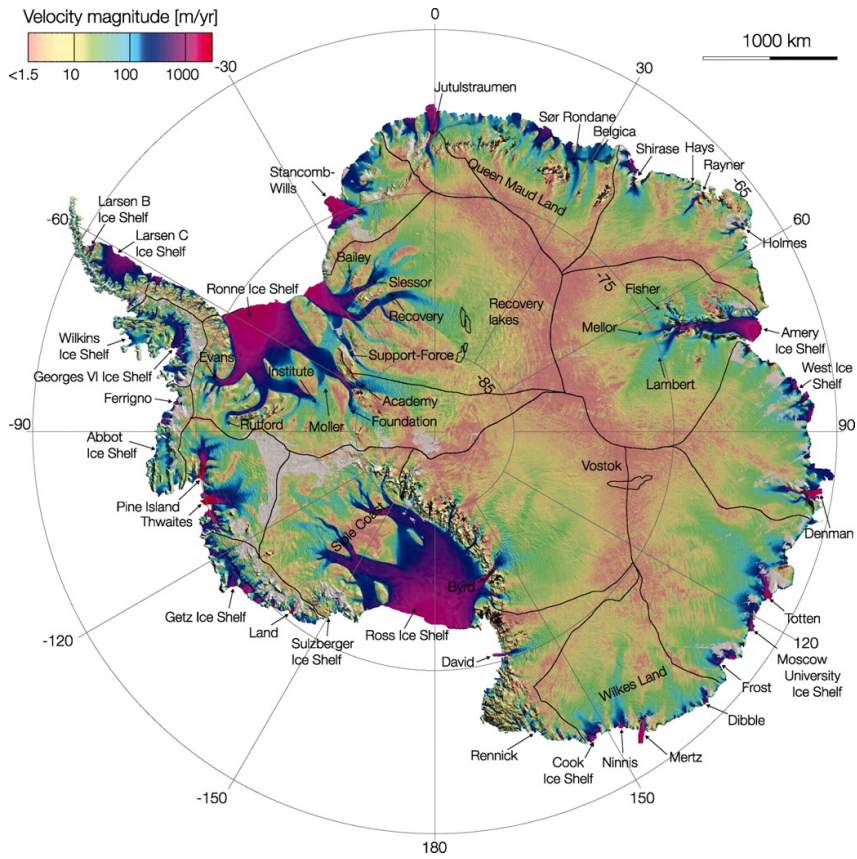


Figure 2.1: Ice flow in Antarctica from Rignot et al. [2011]. West Antarctica is on the left hand side of the figure.

(TG) and Pine Island Glacier (PIG), followed in lesser size by Smith, Kohler, Pope, and Haynes Glaciers. The two other prominent features of the WAIS are the Ronne and Ross Ice shelves ( $360,000 \text{ km}^2$  and  $850,000 \text{ km}^2$  respectively), the two largest of the world. The Ross Ice Shelf is fed by a group of six ice streams (Mercer, Whillians, Kamb and Bindschadler, MacAyeal and Echelmeyer) that extend inland, as far as, 400 km. In terms of mass outflow, in the Antarctic continent most of the ice returns to the oceans in ice streams, ice shelves and glacier tongues. For the

particular case of the WAIS, ice outflow occurs in the glacier tongues of PIG and TG, and the ice streams that feed the Ronne and Ross Ice shelves.

### **2.2.2 Geological Setting**

East Antarctica rests on a Precambrian craton older than 500 Myr that separated from the other southern continents during the Mesozoic fragmentation of the Gondwanaland supercontinent and has remained in the same position for the last 40 Myr [Dalziel and Lawrence, 2001]. West Antarctica is composed of at least four major crustal blocks assembled in the Paleozoic and Mesozoic that have moved relative to each other during the Late Mesozoic breakup of Gondwanaland. Both of these processes created unusually large, extensive crustal areas that thinned and stretched providing a relatively high geothermal flux at the bottom of the ice column. This crust was likely further altered in the Cenozoic by a mantle plume underneath Marie Byrd Land [LeMasurier, 2008], initiating the West Antarctic Rift System and the subglacial volcanism I observe today. Volcanism in West Antarctica may play a key role in terms of mass balance, by generating melting at the base of the ice that helps lubricate the subglacial topography. This lubrication speeds up the flow of the ice system triggering an increase of the output of mass in the oceans. If mass input is insufficient, the glacier could undergo a decrease in volume in order to regain a steady state by retreating its grounding line. An excessive retreat could create an unstable geometric configuration for marine based glacier glaciers like TG and PIG [Rignot and *et al.*, 2002, Schroeder et al., 2013]. Changes in ocean currents can also trigger grounding line retreat [Pritchard et al., 2012].

### **2.2.3 Surface and subglacial topography**

Tectonic processes have given West Antarctica the 'cradle' shape in which the WAIS lies below sea level, with the exception of a few mountain chains in the Marie Byrd Land area near the Amundsen Sea Embayment (ASE), and the Ellsworth Mountains next to the Ronne Ice Shelf [Dalziel and Lawver, 2001]. The complex and extensive subglacial topography includes valley systems, mountain chains and deep trenches, like the Bentley Trench, the lowest point in West Antarctica, at 2550 m below sea level. The configuration of all these features determines the distribution and direction of the regional ice flow systems, that in the case of WAIS, are symmetrically divided in three main drainage sectors (ASE, Ronne and Ross ice shelves), each corresponding roughly to a third of the ice sheet's area with its triple junction located approximately in the center of West Antarctica.

A second important geological control of mass balance in the subglacial realm is the process of sedimentation. Sampling of marine sediments and subglacial till reveals clear evidence that there have been periods of advance and retreat of the WAIS, where at times it was completely absent, having its present position occupied by water, and other periods where its extent reached, as far as, the edge of the continental shelf [Naish et al., 2009].

These sediments originate from marine sedimentations and subglacial erosion during the periods of deglaciation. The till interacts closely with the bottom of the ice column [Blankenship et al., 1986] as when it is saturated with water the till can speed up ice motion and when it is dry or frozen, slow down the ice. Additionally, to serve as a controlling factor of ice movement, the till layer can be

transported along with the flow of ice.

Another related phenomenon at the ice bedrock interface is the increase of the hydrostatic pressure by the influx of water from the ubiquitous subglacial water systems. The increase is due to differences of the hydraulic gradient from place to place. As a result, an increase of water pressure can eventually lift the glacier and make the friction between the ice and the bedrock go to zero, speeding up the glacier [Stearns et al., 2008]. In the case of permanent or semi-permanent subglacial water systems (like a subglacial lake), a localized fast surface velocity could appear as a local anomaly of input and output of ice flow [Hindmarsh, 1998].

A major effect of the differences in subglacial conditions (subglacial topography and distribution and abundance of till material) between West Antarctica and East Antarctica is the shape of their respective ice sheet profiles. For East Antarctica, the profile is almost parabolic, indicating the bulk of ice motion is accommodated by ice deformation, while the profile in most of West Antarctica is convex-up shape close to the ice divide and changing to a concave up downstream and finally to flat as the ice approaches the ice shelves [Bindschadler, 2006b], indicating significant sliding toward the coasts. However, at TG, the profile turns strongly convex-up toward the coast, indicating strong bed coupling as the coast is approached [Joughin et al., 2009, Schroeder et al., 2013].

A particularly important source of ice loss in this region is the circulation of deep warm ocean water to the grounding line level, inducing acceleration by reducing the buttressing resistance of floating ice shelves [Bindschadler, 2006b].

#### 2.2.4 Climate

Up to now, I have described the mass loss component of the mass balance equation for the West and East Antarctic Ice Sheets, which is determined by the ice flow speed at the grounding line and ice thickness. What preserves the ice sheet volume is the replenishment of mass by the process of snow fall (or accumulation). This snow is densified into ice, through the intermediate stage between snow and ice called *firn*. The distribution of this replenishment is a function of ice surface slope, altitude, latitude, and climate variables like air temperature and wind patterns. The accumulation rate is determined by the moisture content of the atmosphere, provided mainly from the surrounding ocean and sea ice [Zwally and Giovinetto, 1997].

The combination of the amount and distribution of accumulation determines the ice flow behavior, along with the hitherto mentioned geological controls of: subglacial topography, subglacial melting, and the distribution and thickness of subglacial till; when one or more of these factors is modified (particularly from climate perturbations), the ice sheet changes its response to internal and/or external forcing in order to readjust its geometrical configuration and reach a new state of balance, a process that changes the distribution of stress and strain fields, and can take millennia [Paterson, 1994].

Accumulation rates are larger in West Antarctica as compared to those in East Antarctica with approximate values of 0.22 m/yr and 0.07 m/yr, respectively [Rignot and Thomas, 2002]. These high accumulation rates can penetrate from the coast further inland than in East Antarctica thanks to the relatively low surface

profile of West Antarctica, resulting in accumulation rates as large as 0.1 m/yr at the ice divide.

The Antarctic climate influences and is influenced by the global climate, of particular importance is mention deserves the El Niño Southern Oscillation (ENSO), an anomaly in the coupling of the Pacific Ocean and the atmosphere at equatorial latitudes that impact the global climate. Its main repercussion in West Antarctica is the oscillation of the Polar Low (a general indicator of the WAIS climate) between the ASE and the Ross Sea. Depending on the position of the Polar Low, the wind system will carry air moisture either to the ASE or the Ross Sea. During the 1980s, accumulation rates in West Antarctica showed a positive correlation with the Southern Oscillation Index, a measure of the strength of the El Niño-La Niña cycle. A recently observed phenomena [Monaghan and Bromwich, 2006] is the antiphase correlation of this pattern with WAIS accumulation rates since 1990. The nature of this shift is not yet understood, but it might imply deeper connections between the Antarctic climate, the ENSO, and perhaps other global climatic processes.

Anomalies in natural climatic fluctuations at different timescales and/or abrupt climate perturbations induce variations in the amount of snow that a glacier collects and the amount of ice lost by calving and melting. These variations initiate a series of complex changes in the ice flow from which the glacier responds by adjusting to a new state of balance throughout a reposition of the grounding line and change of the ice thickness [Paterson, 1994]. For example, an increase in temperature induces an increase in the amount of snow fall because the air is capable of hosting more moisture. This suggests a correlation between the increase in temper-



atures observed since the beginning of the industrial world (1850) and a potential increase in accumulation rates over the Antarctic continent. There have been recent reports of increases in temperatures over the last half century in West Antarctica from both satellite [Comiso, 2000] and ground observations [Steig et al., 2009a,b, Bromwich et al., 2013].

### **2.3 Thwaites Glacier**

Thwaites Glacier (TG) is the second largest glacier of the WAIS, (Figure 2.2) draining an area of approximately 167,000 km<sup>2</sup> that is surrounded at the north by the Amundsen Sea, at the west by PIG and on the east flank by Marie Byrd Land [Rignot and Thomas, 2002]. TG drains a marine ice sheet with its ice bedrock interface well below sea level, and depths deeper than 2000 m and surface elevations higher than 2000 m above sea level [Bindschadler, 2006a]. TG presents a non-parabolic profile that indicates non steady flow. Satellite observations of the last 15 years show a retreating grounding line along with acceleration and thinning of the ice column in the TG sector of fast flow [Rignot and *et al.*, 2002], close to the coast.

In terms of subglacial topography [Holt et al., 2006], the TG catchment is underlain by a single, large deep basin bounded by a broad coastal sill of low topographic relief and fed by a dendritic pattern of deeply incised valleys. All six of the TG tributaries identified by Lang et al. [2004] from ice surface velocities correspond to deep subglacial troughs, yet the TG trunk lies in a very broad trough that may allow for rapid changes in flow geometry. More specifically, the zone of fastest flow in TG is confined by subglacial topography on its western margin;

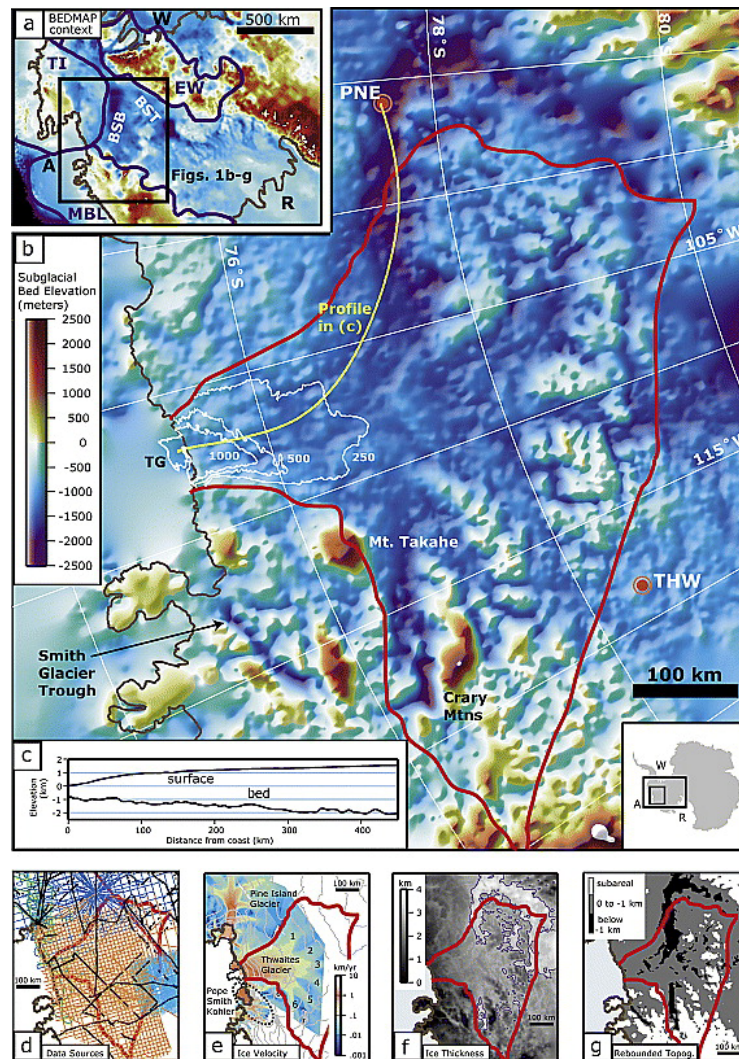


Figure 2.2: Context figure for Thwaites Glacier, from Holt et al. [2006]. a) bed elevation context in West Antarctic [Lythe et al., 2001], b) AGASEA derived bed elevations, c) Surface and bed elevations along the yellow transect in b, d) datasets in this compilation. The dataset used for this thesis is in orange, e) 1996 ice flow velocities from InSAR [Rignot et al., 2003], f) Ice thickness, 3 km contour shown, g) deglaciated topography.

however, topography beneath its eastern margin, while clearly influencing ice flow to some degree (e.g., 250 m/yr contour), lacks such a gradient [MacGregor et al., 2013]. This could be a factor in the apparent widening of fast flow near the TG grounding line [Rignot and Thomas, 2002] and indicates that the fast flow zone could widen further.

## **2.4 Data Acquisition for this Work**

The University of Texas Institute for Geophysics (UTIG) performed in the austral summer of 2004-2005 a comprehensive aerogeophysical survey over the TG (Airborne Geophysics of the Amundsen Sea Area (AGASEA). on a 15 x 15 km grid, yielding over 43,000 line km of data including seven survey lines that follow ice flow lines [Holt et al., 2006]. The UTIG instrumentation included gravity, magnetics, laser ranging, ice penetrating radar and kinematic GPS positioning. The goal of the mission was to measure ice sheet properties, subglacial sedimentation and upper crustal characteristics (among others) with the purpose of analyzing their dynamics and interactions. From the mass balance point of view, key measurements were surface altimetry [Young et al., 2008], bedrock topography [Blankenship and Young, 2012] and englacial layer distribution, with the last two provided by the radar system and the surface topography by the laser altimeter. The analysis and interpretation of the radar data permitted interpretation of two shallow ice layers of volcanic origin that are present throughout the survey. These layers are the primary source of information for determining the distribution of accumulation rates across the entire catchment of Thwaites Glacier, when combined with complementary data

from ice cores and satellite observations of ice surface velocity.

## **2.5 Radar Data Set**

The UTIG ice penetrating radar is a phase coherent radar sounder [Peters et al., 2005, 2007] with a 60 MHz center frequency, transmitting a one  $\mu\text{sec}$  15 MHz chirp (a time variable frequency signal [Soumek, 1999]) at a pulse repetition frequency (PRF) of 6.4 KHz. Two underwing radar antennas were mounted on a Twin Otter traveling at 65 m/sec. Radar returns were sampled at a rate of 20 nsec with coherent integration of 32 signals every 35 cm along the aircraft direction [Holt et al., 2006, Peters et al., 2007]. Mathematically, the resolution of the radar system is given by the width of the radar pulse compression (i.e., the convolution of the radar echo signal and the complex conjugate of a replica of the transmitted signal reversed in time [Soumek, 1999]). The data processing for this analysis gives a resolution of 16 meters in the horizontal direction and about 8 meters in the vertical direction. Because of this resolution a single layer in the radar section represents the averaging of multiple annual layers although, I believe that this bandwidth limited vertical range precision for establishing layer depths is higher as our signal to noise ratio is high.

We processed the radar data by coherently averaging the full waveforms to 20 Hz to reduce the effect of surface scattering through destructive interference, and then finding the amplitude of the signal. These amplitude records were then incoherently averaged to 4 Hz to further reduce improve signal to noise, providing a record every  $\sim 20$  meters.

To interpret layers, I used Schlumberger's GeoFrame IESX seismic interpretation system. Arrays of processed record (radargrams) were adjusted to the surface return, and a scaling factor was used to interpret these record at the  $\mu\text{sec}$  timescales used for radar. These horizons were exported, converted to depths using a constant electromagnetic velocity in ice of  $168 \text{ m}/\mu \text{ sec}$ , and combined with GPS position data to geolocate the layer data.

## Chapter 3

# Millennial scale accumulation rates over the catchment of Thwaites Glacier, Antarctica

### 3.1 Introduction

The West Antarctic Ice Sheet is more susceptible to regional changes than its counterpart, the East Antarctic Ice Sheet (EAIS), because of its lower altitude and higher moisture budget penetrating inland. WAIS accumulation rates are larger than  $0.1 \text{ m yr}^{-1}$  near the divide, three times more than in East Antarctica [Paterson, 1994]. Such large accumulation rates impact WAIS ice flow and mass balance, with a consequent increase in the ice flux to the coast. This high accumulation explains, in part, very large discharge rates for the largest glaciers draining in the WAIS, Thwaites Glacier (TG) and Pine Island Glacier (PIG) [Rignot et al., 2003, van den Broeke et al., 2006].

TG lies in the Amundsen Sea Embayment (ASE) of the WAIS, which is thought to be unstable due to its submarine base and lack of significant buttressing from ice shelves. TG is thus sensitive to external forcing such as changing ocean circulation [Pritchard et al., 2012], modifications to subglacial hydrology [Schroeder et al., 2013] and changing snow accumulation rates, which in turn affect the mass balance of the ice sheet. The present and past distribution of accumulation rates

in the TG catchment are therefore essential boundary conditions needed to drive models of WAIS evolution.

The TG catchment is underlain by a single large, deep basin, bounded by a broad coastal sill of low topographic relief and fed by deeply incised valleys with dendritic drainage patterns that correspond to deep subglacial troughs. The connection between subglacial and surface topographies may be an important control on the spatial distribution of accumulation rates [Spikes et al., 2004].

In this paper, we estimate the accumulation rates from radar detected englacial layers for the entire TG catchment using the local layer approximations (LLA). The LLA is appropriate for areas close to the ice divide where gradients in horizontal ice flow, accumulation and ice thickness tend to be small [Waddington et al., 2007]. To assess change in accumulation over the last few centuries, we compare our centennial accumulation rates with contemporary values of snow fall: the RACMO2.1 atmospheric model [Lenaerts et al., 2012b] and a remote-sensing technique based on a polarization of passive microwave satellite radiometry from the spaceborne Advanced Microwave Scanning Radiometer (AMSR) instrument [Arthern et al., 2006]. From this comparison, we test the hypothesis that accumulation rates have not changed over the last millennium.

## **3.2 Radar Data**

The University of Texas Institute for Geophysics performed an aerogeophysical survey over the catchment of TG on a 15 km x 15 km orthogonal grid using a DHC-8 Twin Otter F-CSJB aircraft, yielding over 43,000 line km of data, includ-

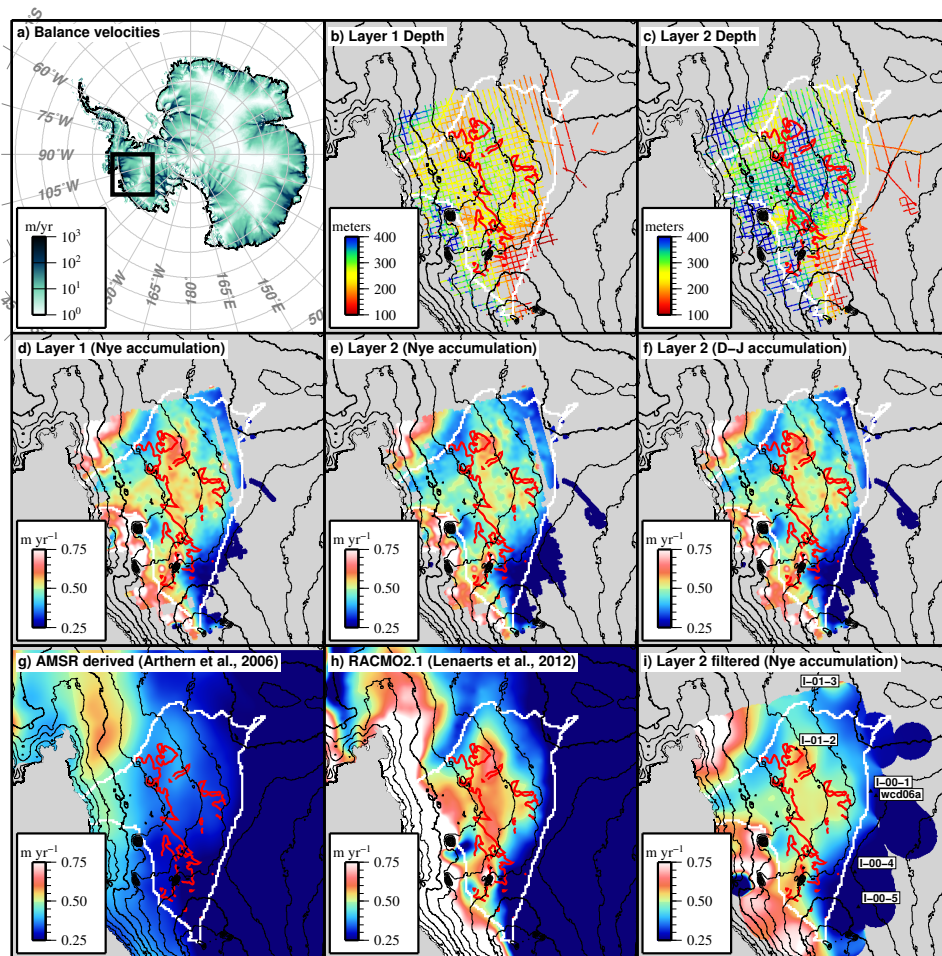


Figure 3.1: Patterns of ice equivalent accumulation in TG: a) location map with balance velocities after Le Brocq et al. [2006]; b) and c) interpreted layer depths (ice equivalent); d) and e) accumulations rates using Nye [1963]; f) accumulation rates using Dansgaard and Johnsen [1969] for lay2; g) remote sensing derived interpolation [Arthern et al., 2006]; h) the RACMO2.1 atmospheric model of precipitation [Lenaerts et al., 2012b]; d) filtered version of e) with ice core locations. In all panels: black contours, surface elevations [Fretwell et al., 2013]; red line, threshold where  $D$  [Waddington et al., 2007] equals 0.5; white line; TG catchment [Vaughan et al., 2001]. Figures 3.2 to 3.8 are expanded versions of these maps.



ing seven along-flow survey lines [Holt et al., 2006]. One of the components of the survey is the HiCARS ice-penetrating radar system [Peters et al., 2005], which allows for the interpretation of bedrock topography [Holt et al., 2006], basal properties [Schroeder et al., 2013], and englacial stratigraphy of the ice [Morse et al., 2002, Carter et al., 2009]. HiCARS operates with a 60 MHz center frequency, transmitting a  $1\ \mu\text{sec}$ , 15 MHz bandwidth chirp at a pulse repetition frequency (PRF) of 6.4 kHz [Peters et al., 2005]. The compressed pulse width is 100 nsec, yielding a resolution in ice of  $\sim 9$  m. The radar data is coherently integrated to 20 Hz, and then incoherently averaged to 4 Hz. Given an average aircraft speed of  $65\ \text{msec}^{-1}$  this processing provided a trace every 17 m along track.

We have tracked the two shallowest, fully-continuous layers through most of the TG dataset (Figures 3.1b,c and 4.4, 4.5 ). The layers are shallower on the divide and deeper close to the coast, where they tend to be untraceable in highly-crevassed areas of fast flow. Near the divide, the layers become too shallow to track, due to coherent pulse compression artifacts from the bright surface radar echo that obscures the top 100 m of the ice column. To obtain the ice equivalent depth of each layer, we use a constant velocity of  $169\ \mu\text{sec m}^{-1}$ ; we use these depths for our catchment wide accumulation modeling (Figure 3.10 and 3.11).

### 3.3 Ice Core Chronologies

We use published ice core chronologies from the ITASE [Kaspari et al., 2004] and WAIS Divide [Sowers, 2010] projects to assess and calibrate our radar data. The ITASE expedition (2000-2001) drilled ice cores traversing most of the

Table 3.1: Ice Cores, Mean Accumulation Values at WAIS, i.e.,  $\text{m yr}^{-1}$

Ice Core	Time Period	Mean, i.e.
ITASE-00-4	1799-2000	$0.206 \pm 0.04$
ITASE-00-5	1716-2000	$0.152 \pm 0.04$
ITASE-00-1	2001-2002	$0.327 \pm 0.03$
ITASE-01-2	1890-2001	$0.46 \pm 0.09$
ITASE-01-3	1859-2001	$0.35 \pm 0.08$
WDC05A	1775-2005	$0.218 \pm 0.04$
WDC05Q	1521-2005	$0.218 \pm 0.04$
WDC06A	1900-1999	$0.218 \pm 0.04$

WAIS sector, with TG and Pine Island Glacier (PIG) containing cores 01-2, 01-3, 01-5, and 01-06 for the drainage system, and 00-4 and 00-5 close to the ice divide. The WAIS Divide project (2005-2011) drilled the ice cores WDC05A, WDC05Q, and WDC06A over the ice divide, which separates the Ross and Amundsen Sea sectors [Sowers, 2010]. Kaspari et al. [2004] analyzed the ITASE accumulations for the period 1922-91 as an assessment of present-day accumulation rates. These results are summarized in Table 3.1 (adapted from Kaspari et al. [2004] and Lamarque et al. [2010]).

The other ITASE cores were not drilled over our study area, so we cannot perform a direct numerical comparison. Still, we can use them for a qualitative comparison, despite the local variability of surface topography, at the core sites, and local climate at 200 km scale [Kaspari et al., 2004], their accumulations indicate close agreement with our results, especially from sites 00-4 and 00-5 at the east-most sector of TG.

### **3.4 Firn Correction**

To make appropriate depth estimates for calibrating against ice cores, it is necessary to correct for variable electromagnetic wave speed in the ice column due to changes in density through the firn depth [Paterson, 1994]. Radar signals travel faster through the less-dense firn (400 to 800 kg/m<sup>-3</sup>) than through ice. The firn layer therefore acts to bias radar layer depths that were calculated using a single velocity for the full ice column. To correct for this bias, we compute a firn model from the ice core WDCO06A, to later calculate age of layers (next section).

From the WDCO06A depth-density profile [Sowers, 2010], we compute the velocity as a function of density [Peters et al., 2005], at each location, to obtain one way travel time (OWTT) between pairs of depth measurements, from here we compute the accumulated OWTT as a function of depth, we compare this result with the ice equivalent depth of a theoretical signal. The differences between the two results is the firn correction at the location of the ice core.

As the WDCO06A profile does not reach the depth of layer 2, we determine fitting a fifth order polynomial in order to extrapolate the corresponding depth. As density does not vary significantly below layer 1, we find firn corrections of 9.5 meters for both layers.

### **3.5 Age of Layers**

For the AGASEA dataset, our closest layer data is 5 km from the WDCO06A ice core site. However, the WAIS Divide site was overflowed five years later during

a transit for the ICECAP project with a similar HiCARS radar system [Blankenship et al., 2014]. The layers were identified in this record and our firm correction was applied to the ice equivalent depths to find the physical depth of each reflector.

With the fitted depth as a function of the integrated OWTT from the previous section, I determine the methane gas age versus depth [Sowers, 2010] for layer 1 and layer 2 respectively, using:

$$T = T_g + C + (2004 - 1950) \quad (3.1)$$

where  $T$  is the age of the layer in years,  $T_g$  is the measured age of methane at a given depth,  $C$  accounts for the gas age – ice age difference of 208 years, [Sowers, 2010], and 2004 and 1950 are the years of our data collection and the ice core age-scale reference. At this location, depths and ages for layer 1 and layer 2 are determined to be  $143 \pm 4.5$  m ( $548 \pm 20$  yr) and  $188.5 \pm 4.5$  m ( $725 \pm 20$  yr) respectively.

The dates of these layers are between 1437 CE to 1477 CE for layer 1 and 1259 CE to 1299 CE for layer 2. We attribute layer 1 to the globally observed sulphate peak due to the 1459 CE Kuwae, Vanuatu, eruption event [Sigl et al., 2013] and layer 2 corresponds to a similar 1257 CE peak that may be tied to an eruption at Samalas Volcano, Indonesia [Lavigne et al., 2013]. The strong correlation of the volcanic dates and the center estimate for the layer depths (a difference of 2 years for each layer) suggests the depth precision of each layer is much better than the bandwidth limited resolution of the radar.

## 3.6 Models

### 3.6.1 Nye Model

Annual layers of ice accumulation thin as a consequence of compression by subsequent snowfall and stretching in the horizontal direction, which is produced by sliding of ice over a tilted bedrock. As a result, accumulation and ice deformation are correlated in a non-trivial manner. In order to directly deconvolve them, one should know the detailed history of accumulation and the stress-strain relation of ice. Additionally, because layers at depth are not always parallel to the surface, shear in the plane parallel to the surface also contributes to thinning [Paterson, 1994]. To simplify this problem, Nye [1963] suggested a relationship for accumulation rates as a function of the age-depth profile which, under a steady state assumption, suggests that accumulation at the surface is compensated by a thinning rate constant with depth [Fahnestock et al., 2001]. This is an unrealistic assumption for the case of a non-frozen bedrock, but valid in shallow layers with little deformation. In this paper I apply two versions of the Nye equation: Nye [1963] and Dansgaard and Johnsen [1969]. The Nye model states:

$$t = -\frac{h}{b} \ln\left(\frac{z}{h}\right) \quad (3.2)$$

where  $h$  is ice column thickness,  $z$  is elevation of a layer above the bed, and  $t$  is layer age obtained from ice cores. Equation 3.2 assumes: (a) a constant vertical strain rate that balances the overburden of local accumulations, (b) layers have uniform thickness, and (c) ice is frozen to the bed [Nye, 1963]. Nye's methodology

implies that thinning is produced by gradients in sliding velocity concentrated at the bed [Fahnestock et al., 2001].

The drawback of the Nye approach is that if the ice is assumed frozen at the bed vertical strain rates in layers close to the bed should be close to zero, implying that the strain rate is zero everywhere. Due to this shortcoming, Nye's approach is valid only in the upper part of the ice column [Paterson, 1994]. The method fails at locations where melting is present at the base creating a layer of water which reduces friction and makes ice flow more easily, leading internal layers to stop thinning. In this instance, there is no need for the overlying layers to deform to compensate the overburden produced by snowfall. Therefore, the age-depth relation of 3.2 is no longer valid [Fahnestock et al., 2001]. The Nye method does not correct for other sources of noise in accumulation such as: divergence/convergence of ice, wind erosion and rapid flow associated with steep bedrock topography, in future work I will deal with these additional sources of error.

### **3.6.2 Dansgaard-Johnsen Model**

Nye's model assumes a constant vertical velocity throughout the ice column, with all vertical deformation concentrated on an infinitesimal layer at the bottom of the ice, a useful but rarely realistic approximation. A more sensible model by Dansgaard and Johnsen [1969] treats ice as deforming at a maximum constant vertical strain rate from the surface down to some depth  $h'$ , known as the shearing layer. Below this critical depth, deformation drops linearly to zero at the ice-bedrock interface, which implies that ice age and accumulation rate are related by:

$$t = \frac{(2h - h')}{2b} \ln \left[ \frac{(2h - h')}{(2z - h')} \right] \quad (3.3)$$

where parameters are analogous to those in the Nye model. Our values of  $h'$  are based on those used by Neumann et al. [2008] which assumes  $h' = 0.2h$  (where  $h$  corresponds to ice thickness), in areas close to the ice divide. Assumptions for this model include constant flow and accumulation rates and that horizontal deformation has not thinned the layers significantly.

### 3.7 Results

Accumulation rates in TG follow the general pattern of precipitation for an adiabatic lapse rate regime: high values of accumulation rates in areas close to the ocean and a decreasing accumulation trend toward inland, high-altitude sectors, reaching minimum accumulation values at the ice divide with average values of  $0.8 \text{myr}^{-1}$  and  $0.2 \text{myr}^{-1}$  ice equivalent (i.e.), respectively. The Nye and Dansgaard-Johnsen (D-J) methods agree closely (Figures 3.5,3.6) because the layers in this study are shallow enough to be above the shear layer  $h'$ , a zone where the two methods are equivalent [Paterson, 1994].

Compared to the inland-decreasing accumulation pattern, TG presents two significant anomalous features in accumulation rates. First, a zone with greater accumulations on the onset of fast flow, and second, an area of low accumulation at the north-east flank, at the margin of PIG (Figure 3.1 ,3.4,3.5 ). The first anomaly is a consequence of the transition from stagnant to fast flow where changes in bedrock

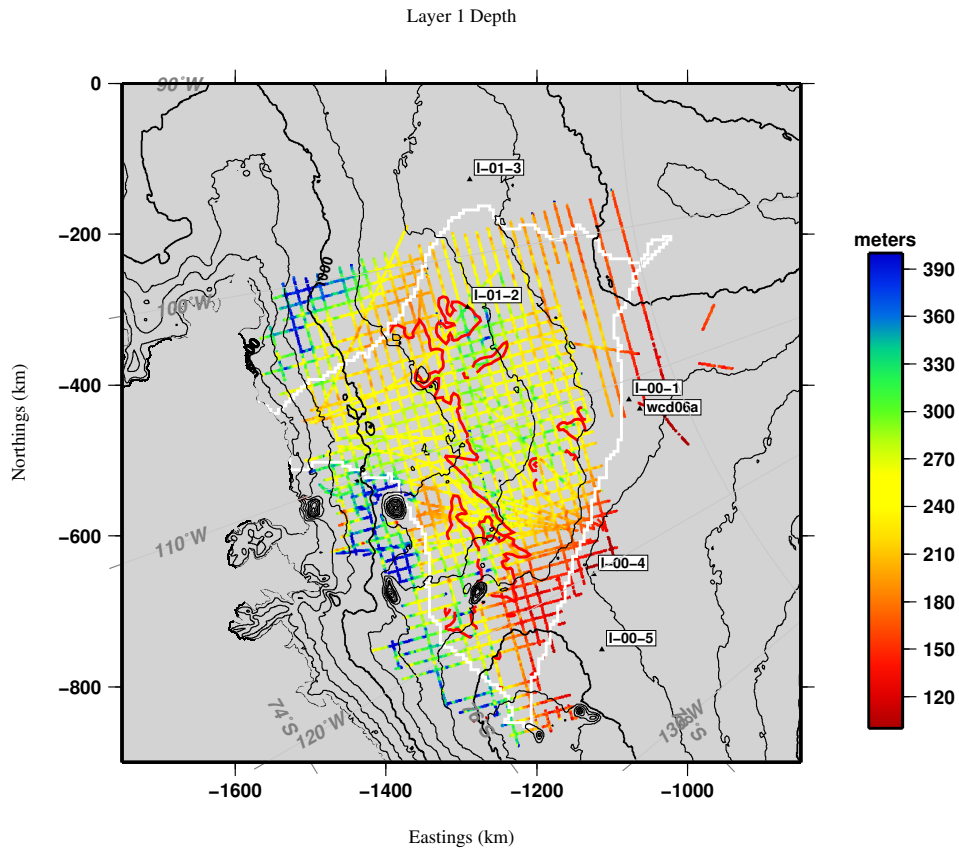


Figure 3.2: Ice equivalent depth for layer 1. Black contours, surface elevations [Fretwell et al., 2013]; red line, threshold where  $D$  [Waddington et al., 2007] equals 0.5; white line; TG catchment [Vaughan et al., 2001].

slope go from tilted to relatively flat, causing a pile up of ice which results in increased snow deposition. Additionally, a change in ice flow regime from simple shear to compressional deformation could result in thicker layers than in the surrounding areas. The second anomaly is a result of an unusual pattern of wind erosion along the ice divide, with winds flowing to either side of the divide. In other words, an orographic effect induces low values of accumulation in the coastal areas.



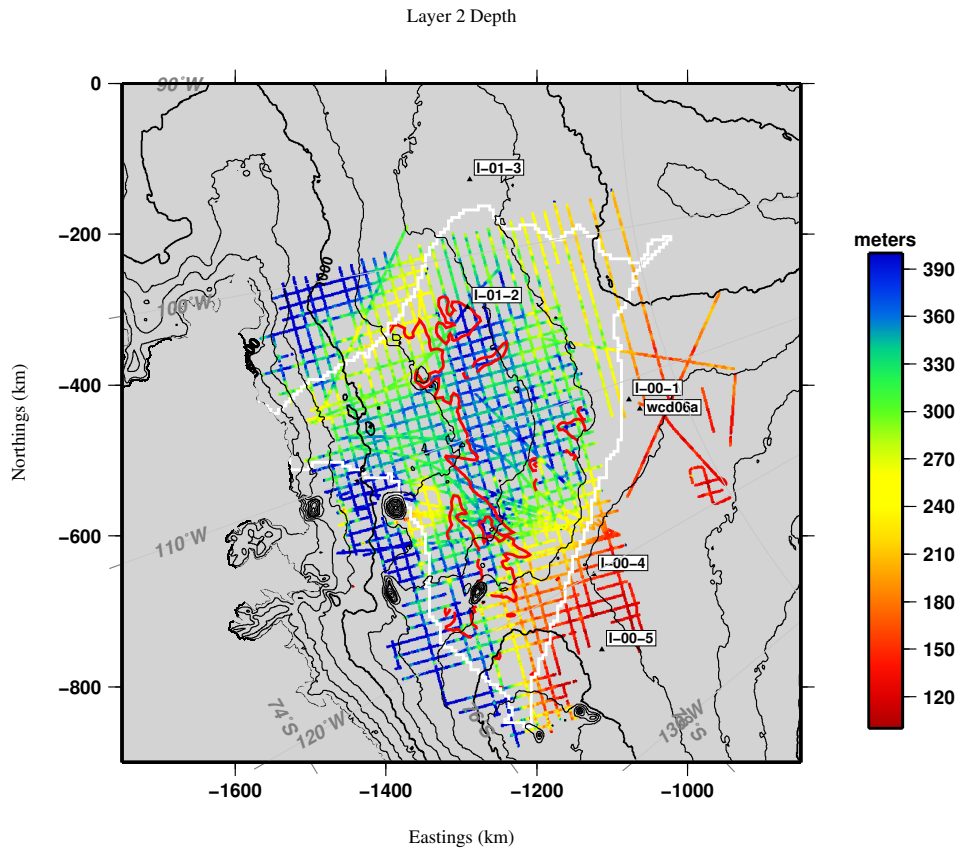


Figure 3.3: Ice equivalent depth for layer 2. Black contours, surface elevations [Fretwell et al., 2013]; red line, threshold where  $D$  [Waddington et al., 2007] equals 0.5; white line; TG catchment [Vaughan et al., 2001].

To evaluate temporal patterns in TG, I compute the difference between accumulations from layers 1 and 2. If all the factors that influence accumulation rates (such as climate, moisture budget, ice flow dynamics and orographic features) remain the same over the lifetime of the layers, this difference should be zero independent of whether or not the glacier is in steady state. A positive difference between the older and the younger layers may indicate areas of localized subglacial

Layer 1 (Nye accumulation)

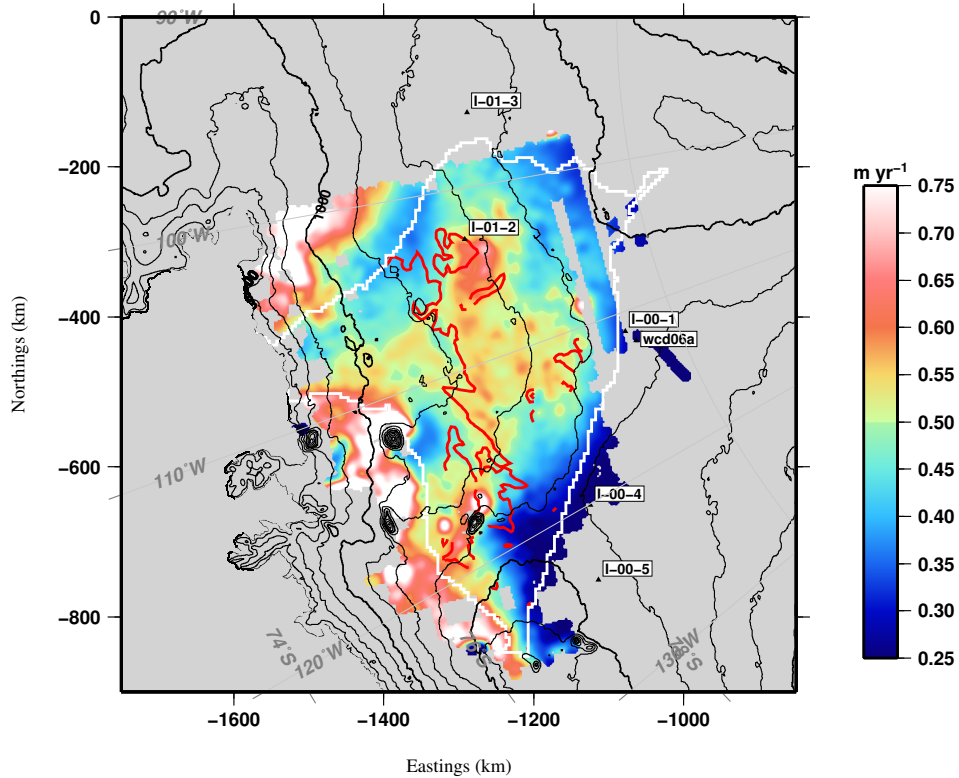


Figure 3.4: Nye inferred ice accumulation rates for layer 1. Black contours, surface elevations [Fretwell et al., 2013]; red line, threshold where  $D$  [Waddington et al., 2007] equals 0.5; white line; TG catchment [Vaughan et al., 2001].

melting which could hint at recently-active subglacial volcanoes in the middle of TG near ice core I-01-2 (Figures 3.1 , 3.5 ).

We do not attempt an analysis of random fluctuations on localized spatial scales (less than 200 km) due to constraints of resolution [Spikes et al., 2004]. Despite the fact that I observe locally high accumulation rate anomalies, I do not expect to associate them with a local climate signal. Rather, I relate them spatially

Layer 2 (Nye accumulation)

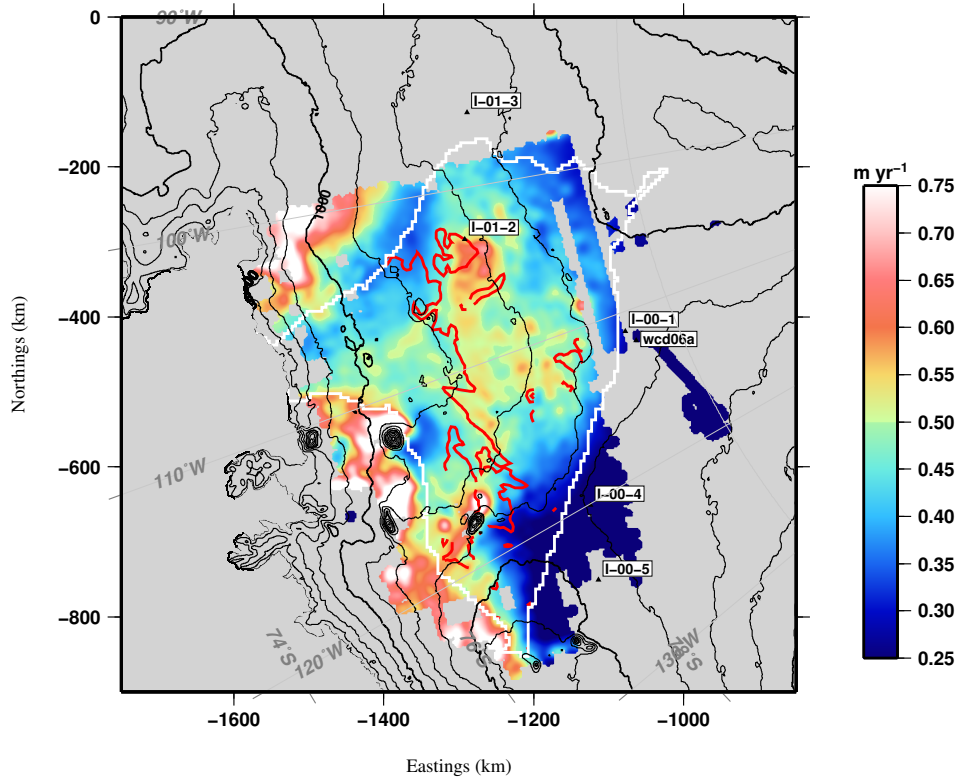


Figure 3.5: Nye inferred ice accumulation rates for layer 2. Black contours, surface elevations [Fretwell et al., 2013]; red line, threshold where  $D$  [Waddington et al., 2007] equals 0.5; white line; TG catchment [Vaughan et al., 2001].

to orographic features of surface topography and subglacial conditions such as basal melting, with the latter hinting at the potential presence of subglacial volcanoes of which examples are suspected in this region [Lough et al., 2013, Behrendt, 2013].

Layer 2 (Nye accumulation)

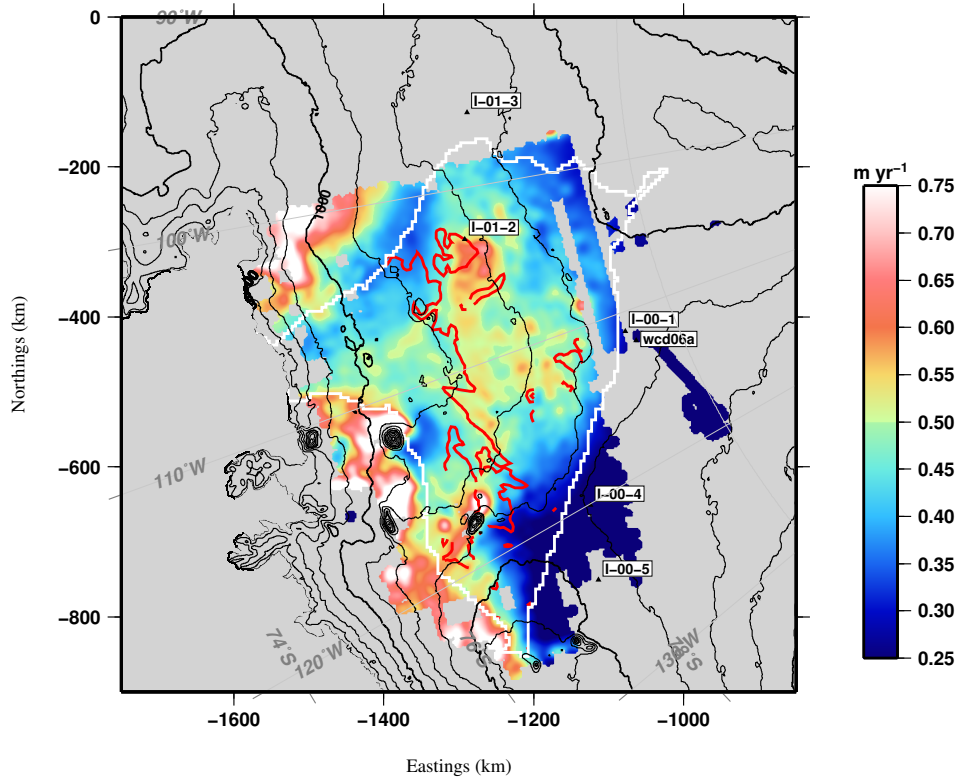


Figure 3.6: Dansgaard-Johnsen inferred ice accumulation rates for layer 2, using a  $h'$  of 0.2. Black contours, surface elevations [Fretwell et al., 2013]; red line, threshold where  $D$  [Waddington et al., 2007] equals 0.5; white line; TG catchment [Vaughan et al., 2001].

### 3.8 Comparison of Long Term and Modern Accumulation Rates

As stated before, the comparison of our centennial accumulations to present rates of snowfall is of interest, for studies of glacier mass balance as well as interactions with climate and ocean forcing. Observations have reported a recent trend of increasing temperatures in ASE and the coastal areas of the Antarctic Peninsula, which suggests that accumulation rates have increased since the beginning of

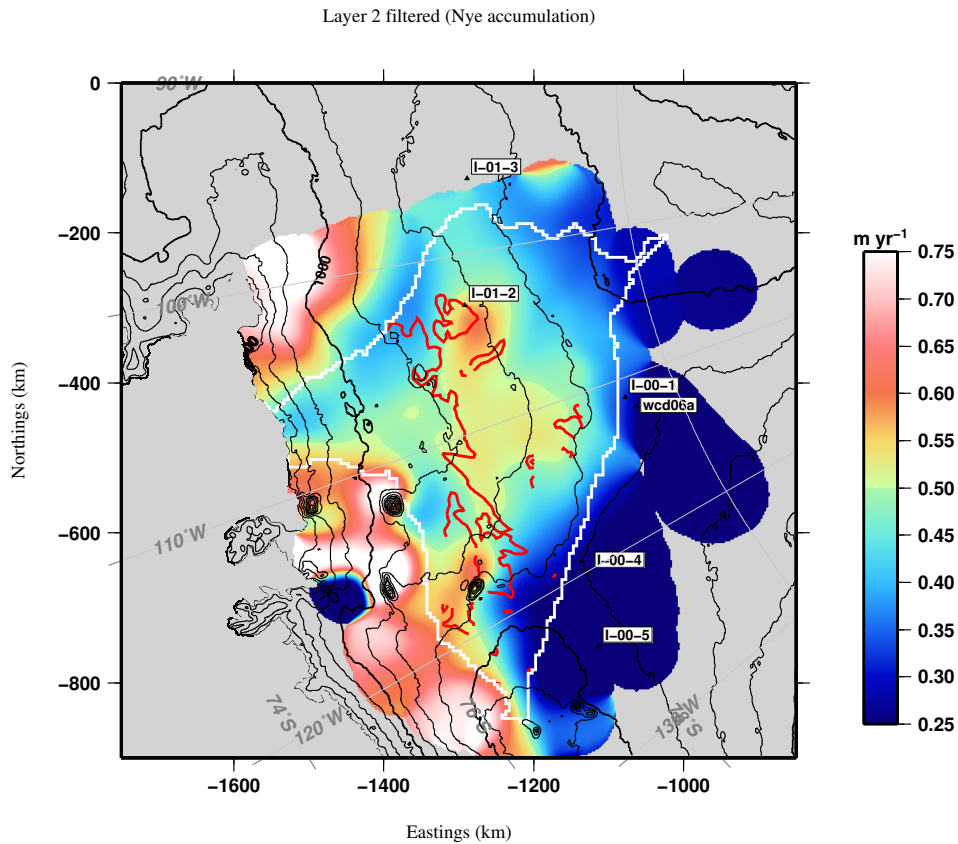


Figure 3.7: Filtered Nye accumulation for layer 2, over 30 km for comparison with models of accumulation. Black contours, surface elevations [Fretwell et al., 2013]; red line, threshold where  $D$  [Waddington et al., 2007] equals 0.5; white line; TG catchment [Vaughan et al., 2001].

the industrial era [Vaughan et al., 1999]. However, such a change has not been observed.

We compare our results with ice cores ITASE-01-1 [Kaspari et al., 2004] and WDC06A [Sowers, 2010], and ITASE-01-1, and two contemporary estimates of snowfall precipitation: AMSR [Arthern et al., 2006] and RACMO2.1 [Lenaerts et al., 2012b],

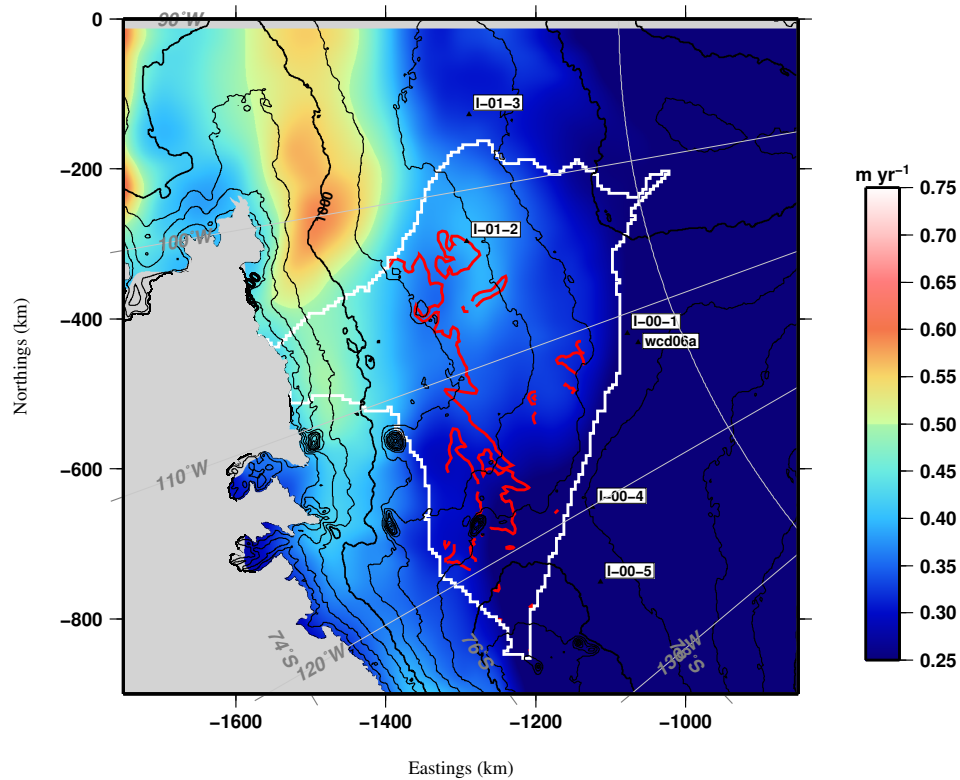


Figure 3.8: AMSR interpolation of surface measurements [Arthern et al., 2006]. Black contours, surface elevations [Fretwell et al., 2013]; red line, threshold where  $D$  [Waddington et al., 2007] equals 0.5; white line; TG catchment [Vaughan et al., 2001].

### 3.8.1 RACMO2.1 and AMSR Derived Accumulation Estimates

We apply a gaussian filter with a width of 30 km ( $\sim 6$  times the ice thickness) to our Nye accumulation rates for comparison to the lower resolution model and remote sensing data. Figures 3.1g,h and i (expanded as Figures 3.7, 3.8, and 3.9) show that all models demonstrate the same large-scale patterns of accumulation in the interior of the ice sheet. However, fine resolution discrepancies exist

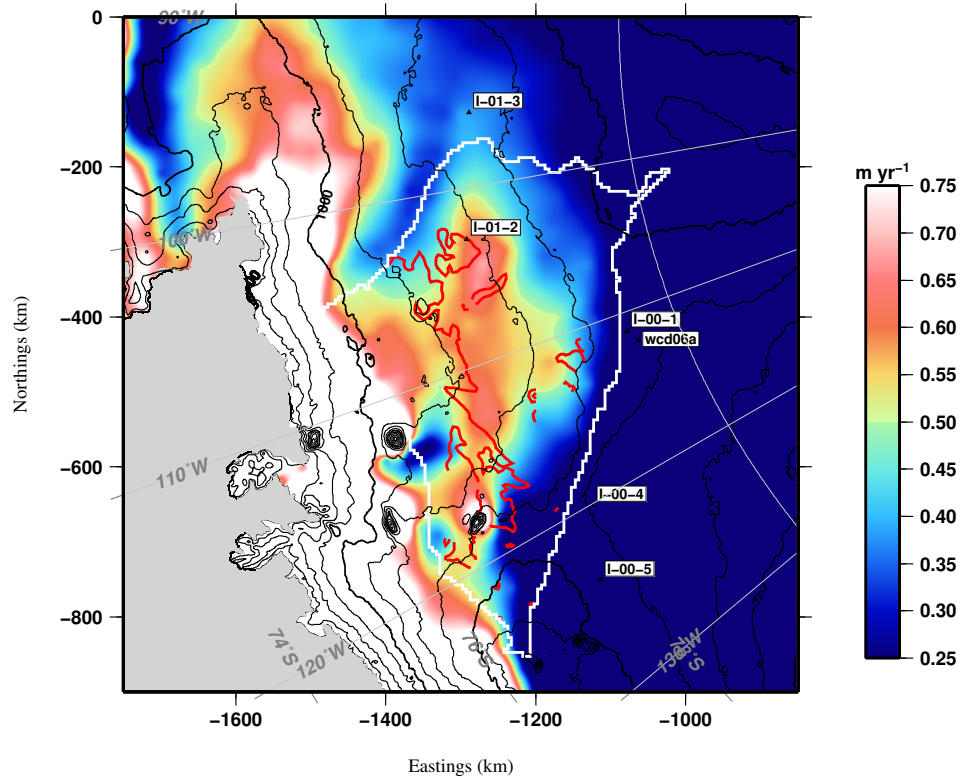


Figure 3.9: RACMO 2.1 ice accumulation rates [Lenaerts et al., 2012b]. Black contours, surface elevations [Fretwell et al., 2013]; red line, threshold where  $D$  [Waddington et al., 2007] equals 0.5; white line; TG catchment [Vaughan et al., 2001].

between them that can be explained as a result of differences in model resolution, model physics, and data processing among other reasons. Since both RACMO2.1 and AMSR are low-resolution fields, they do not resolve more localized accumulation patterns, like the one observed at Mount Takahe. Similarly localized areas of basal melting on the scale of 5 km to 10 km will not be resolved by these models.

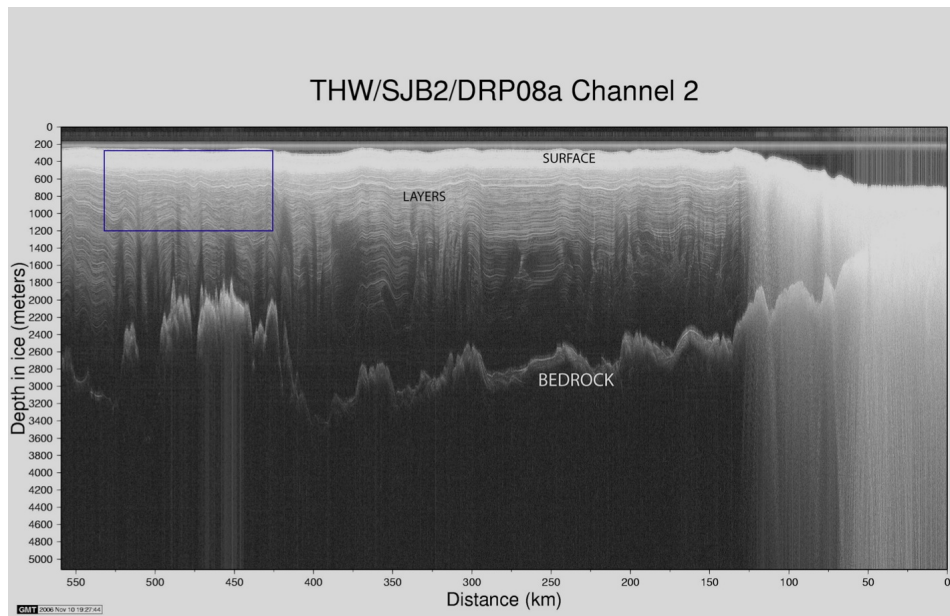


Figure 3.10: Radargram along a flowline showing major features like surface, bedrock topography, englacial layers. Ice divide is at the left, and grounding line at the right. Notice the lack of illumination at the grounding layer produced by heavy crevasse formation. Box indicates shallow layers

### 3.8.2 Ice Cores ITASE 01-1 and WDC06A

Table 3.2 shows that Nye and D-J accumulations both equal  $0.26 \text{ myr}^{-1}$  for layer 1, a difference of  $0.06 \text{ myr}^{-1}$  with respect to WDC06A, an acceptable result given the differences in scale and resolution between the ice core and the radar data, and therefore fairly acceptable (similar analysis holds for layer 2). This result gives us then confidence in our use of the simplified accumulation models, at least in areas of minimal horizontal ice flow; AMSR derived accumulation is even closer to the ice core, whereas RACMO2.1 accumulations are far below to those of the other two models.



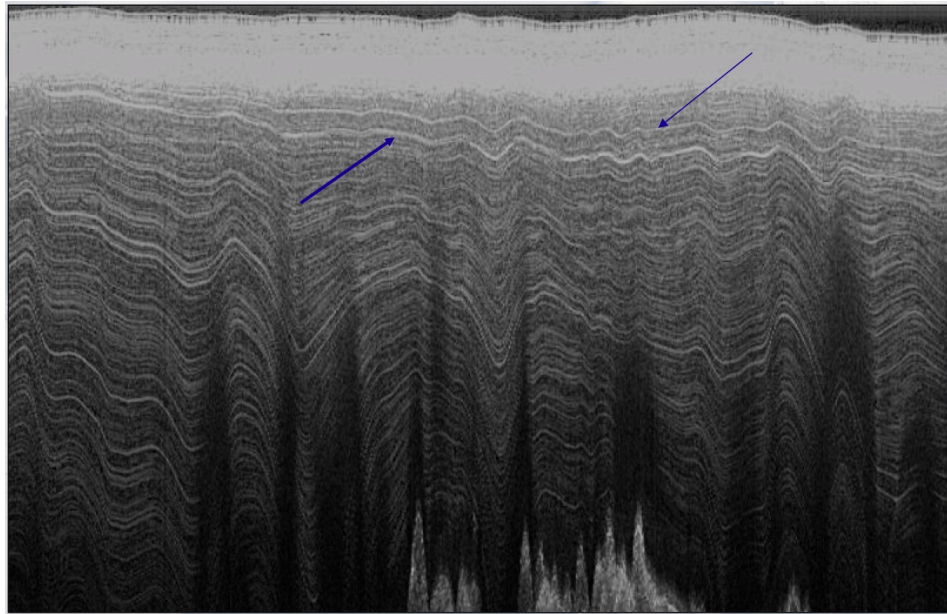


Figure 3.11: Radargram zoom. Arrows indicate layers used for this work. Upper layer is called layer 1, and deeper layer is called layer 2

Results in ice core ITASE 01-1 are not as close as those for WDC06A 3.2;, possible explanation is a larger distance from the divide or possible explanation is a higher influence of local climate [Kaspari et al., 2004]. Ice core ITASE 01-2 is located on the main trunk of TG, but I do not include it in our analysis, as it is located in an area that appears to be influenced by basal melting [Schroeder et al., 2013]. Our results agree qualitatively with accumulation rates at ITASE sites 00-4 and 00-5, in the western most sector of TG (See Table 3.1 and Figure 3.1).

Table 3.2: Accumulations Values at WDCO6A and ITASE-01-1

Accumulation, ice equivalent, $\text{m yr}^{-1}$		
	WDCO6A	ITASE-01-1
	$0.218 \pm 0.04$	$0.327 \pm 0.03$
Nye layer 1	$0.26 \pm 0.02$	$0.393 \pm 0.02$
D-J layer 1	$0.26 \pm 0.02$	$0.371 \pm 0.02$
Nye layer 2	$0.25 \pm 0.02$	$0.395 \pm 0.02$
D-J layer 2	$0.26 \pm 0.02$	$0.373 \pm 0.02$
RACMO2.1	$0.16 \pm 0.03$	$0.381 \pm 0.03$
AMSR	$0.20 \pm 0.04$	$0.303 \pm 0.04$

### 3.8.3 Accumulation as a Function of Elevation

Following Medley et al. [2013], I compute accumulation rates for our results as well as RACMO2.1 and AMSR derived as a function of altitude, every 50 meters vertically. Figure 3.12 shows that radar accumulations and RACMO2.1 agree fairly consistently, both in magnitude and variability at the center of the main trunk, but differ near the coast and in the ice divide. RACMO2.1 underestimates at the divide and conversely overestimates accumulations near the coast. AMSR derived accumulations underestimate accumulations consistently throughout the catchment, but is reliable at least near the ice divide, as validated by WDCO6A. Comparison of our results with the altitude range analyzed by Medley et al. [2013] (1000 m to 1800 m) shows the two are consistent with RACMO2.1.

Average accumulation rates are lower using our method because I integrate

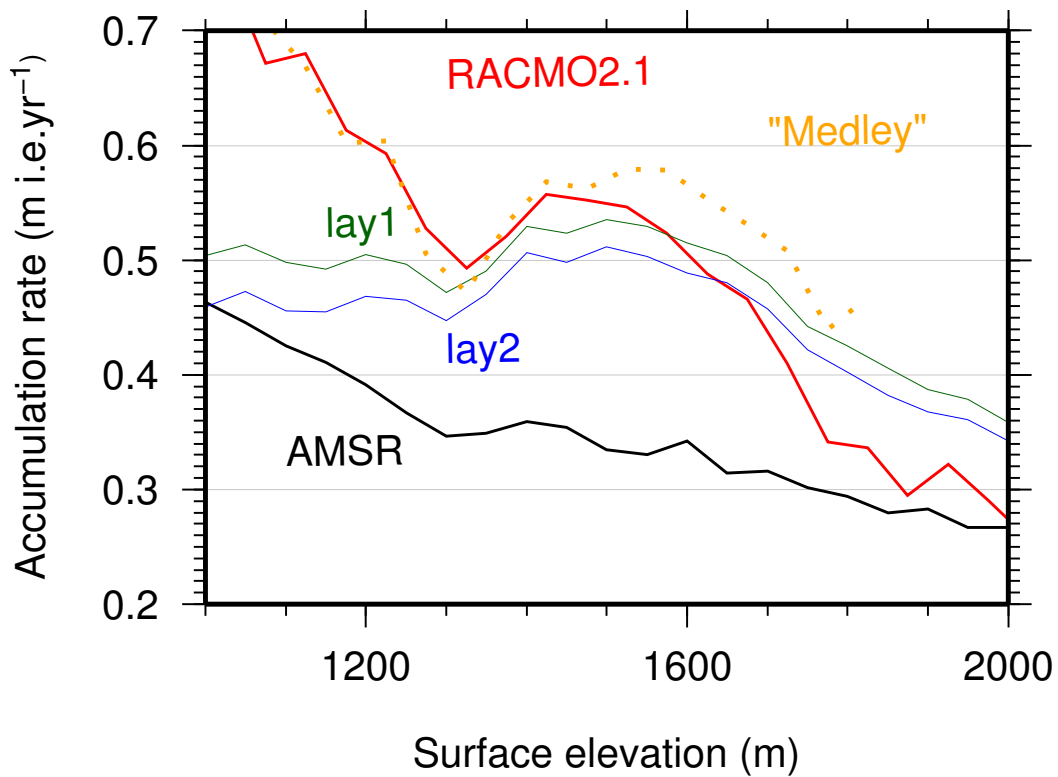


Figure 3.12: Accumulation rates averaged over 50 m elevation bins, integrated over the entire catchment. Given the sparser coverage in Medley et al. [2013], we do not directly compare those results to ours, but instead add their deviation between RACMO2 and the snow radar result to the full catchment RACMO numbers.

over a larger spatial area of the catchment, which includes systematically lower accumulations along the ice divide. Despite this difference, the functional relationship between accumulation rate and elevation is the same in the two methods despite differences in depth, timescale and spatial extent of the study areas used here and in Medley et al. [2013]. We are therefore confident in the robustness of our result that accumulation rates in the TG catchment have not changed over the last 700 years. The above statement does not hold for altitudes below 1200 m, where RACMO2.1

has values larger than Nye and D-J, this is because their assumptions are not longer valid for the corresponding stress/strain field of ice at this altitude and below, where a different flow regime holds. This is confirmed by our computation of the " $D$ " parameter [Waddington et al., 2007], an empirical estimate of where Nye and D-J models are no longer valid because excessive ice deformation. We use as input the BEDMAP2 dataset [Fretwell et al., 2013], MEaSURES velocity data [Rignot et al., 2011] and RACMO2.1 accumulations [Lenaerts and van den Broeke, 2012] to estimate  $D$ , and use a  $D$  of 0.5 as a threshold for ice deformation (Figure 3.1). For our particular case, the threshold  $D$  is reached at the surface topography equal to 1200 m, approximately where our accumulation models no longer agree with RACMO2.1. In future work I will account for the effects of ice flow, where I expect accumulations be closer to RACMO2.1.

### 3.9 Discussion

As mentioned before, TG follows the usual trend of snow precipitation, with the long-term accumulation trend decreasing inland from the coast to the ice divide, with values ranging between  $\sim 1.3 \text{ m yr}^{-1}$  on slow moving ice by Mt. Takahe and  $\sim 0.22 \text{ m yr}^{-1}$  on the divide, with an average of  $0.47 \text{ m yr}^{-1}$  for the the whole catchment. Besides the general trend in precipitation, another distinctive feature in accumulation rate is the relatively sharp increase in accumulation near the onset of fast flow, at the top of the dendritic patterns in subglacial topography (Figure 3.1) . Here in the middle of the ice catchment, accumulation jumps from  $\sim 0.3$  to  $\sim 0.5 \text{ m yr}^{-1}$ . We observe accumulation anomalies related to the geometrical configuration of TG

as follows:

1. The northern-most section of TG presents a boundary of contrasting low and high accumulations with a semi-arc shape, that traverses the zone of fast flow in the SE-NW direction, at the boundary between PIG and TG (Figure 3.1). This boundary corresponds to the location of the shear margin located between the area of fast flow and a zone of relatively stagnant ice. The transition from low to high accumulation is produced by a combination of orographic controls on wind patterns and possibly an influence of a strong circumpolar vortex, which leads to a decrease in accumulation rates by  $\sim 30\%$  in West Antarctica [Neumann et al., 2008].

Between two contemporary accumulation estimate models, RACMO2.1 and AMSR (Figure 3.1) the AMSR-derived method is the only one that tracks the boundary of the shear margin, with the caveat that its values are relatively low for a coastal area. In RACMO2.1, the shear margin boundary is not identifiable, mainly because its resolution is unable to capture this type of regional feature.

2. Another strong anomaly in accumulation occurs in the vicinity of Mount Takahe (Figure 3.1), where zones of low and high accumulations are seen on opposite sides of the volcano. This pattern corresponds to the process of adiabatic cooling: a parcel of humid air hits an orographic barrier where its humidity content is depleted as it rises along the barrier before emerging dryer at the other side of the peak.

3. In the middle of the ice catchment, at the onset of the fast flow (Figure 3.1) I observe a cluster of four bullseye-shaped anomalously high accumulation spots, with values above  $\sim 0.70 \text{myr}^{-1}$  surrounded by accumulations of  $\sim 0.30 \text{myr}^{-1}$ . Given the shape of these features, I hypothesize that this is not an atmospheric feature creating thick layers, but rather a potential indication of melting associated with subglacial lakes [Schroeder et al., 2013].

### 3.10 Conclusions

We compute accumulation rates from radio-echo soundings for the catchment of TG in West Antarctica. Our results indicate accumulation rates ranging from  $0.22 \text{myr}^{-1}$  at the ice divide to  $> 0.80 \text{myr}^{-1}$  at the the coast of the WAIS. Our millennial scale results agree with contemporary independent measurements of snowfall, with the advantage that our survey design is tailored to better capture ice flow conditions in the catchment as well as provide better resolution than the RACMO2.1 and AMSR derived approaches. Comparisons with ice cores from the ITASE and WAIS Divide expeditions show, considering the differences in scale, fairly close agreement in accumulation rates overall with a difference of  $0.06 \text{myr}^{-1}$  i.e. between ice cores and our results, which give us confidence in our methodology and assumptions.

Based on the above I note that, at the scale of our survey, accumulation rates have not changed significantly in the TG catchment since the beginning of the industrial era. However, I still observe a dependence of apparent accumulation rates on areas of fast flow. Nonetheless, I believe our results serve as the best *a*

*priori* information for future models of ice flow dynamics over the majority of the TG catchment.

In future papers, I will assess the effects of horizontal ice flow on accumulation rates for the TG trunk, which will allow for a reassessment of the contribution of TG to sea level rise.

---

## Chapter 4

# Paleoaccumulation rates over the fast flow area of Thwaites Glacier using a flux based method

### 4.1 Introduction

Estimating accumulation rates is of paramount importance in glacier studies because accumulation is one of the main forcing parameters that determines behavior of ice sheets and their state of mass balance. Mass balance of ice sheets is a contributing factor for sea level rise as well as a fundamental variable for climate and ocean models.

Several forcing parameters, both internal and external, influence the balance of an ice mass: surface altitude, latitude, air moisture content, wind distribution, surface temperature, ocean temperature at the grounding line, thickness of the basal till layer, and horizontal and vertical ice velocity, among others.

For the case of Thwaites Glacier (TG) in West Antarctica, anomalously high surface velocities have been observed – as large as 2.5 km/yr at the trunk and approximately 3.8 km/yr at the ice tongue (Figure 4.1, Rignot et al. [2011]). These high velocities impact the mass balance of the ice sheet and enhance internal deformation of the ice to accommodate changes in accumulation and ablation. This can be seen in the equations of mass balance and glacier equilibrium, which are a



function of velocity and mass input.

Here, I will compute accumulation rates for two ice layers (ages  $548 \pm 20$  yr and  $725 \pm 20$  yr) as a function of ice flux along flow lines by expressing them as a function of InSAR surface velocities [Rignot et al., 2011] and assumed values of ice density, including corrections for firn densification and divergence/convergence along flow lines. Leuro et al. [in review] calculate accumulation rates as a function of vertical strain rate, which was held constant to the depth of the shear layer, following the Nye and Dansgaard-Johnsen methodologies. This approach is adequate near the ice divide, but not for areas of fast flow.

We blend the Nye method with an ice flux method by Reeh [1988] in the region of fast flow near the grounding line in order to present a more comprehensive model of accumulation rates. We compare our accumulation results with existing climate models of present-day snow precipitation to validate our results and determine if current and centennial accumulation rates have changed significantly over the past millennia.

Data collection, data processing, and layer interpretation from radio echo soundings are described in detail in Leuro et al. [in review].

## **4.2 Methodology**

Ice flow is a combination of two factors: basal sliding over bedrock and internal deformation of ice mass induced by gravity, with the latter manifesting as an alteration of the equilibrium of the stress-strain field. According to Nye [1958]

InSAR ice velocities (Rignot et al., 2011)

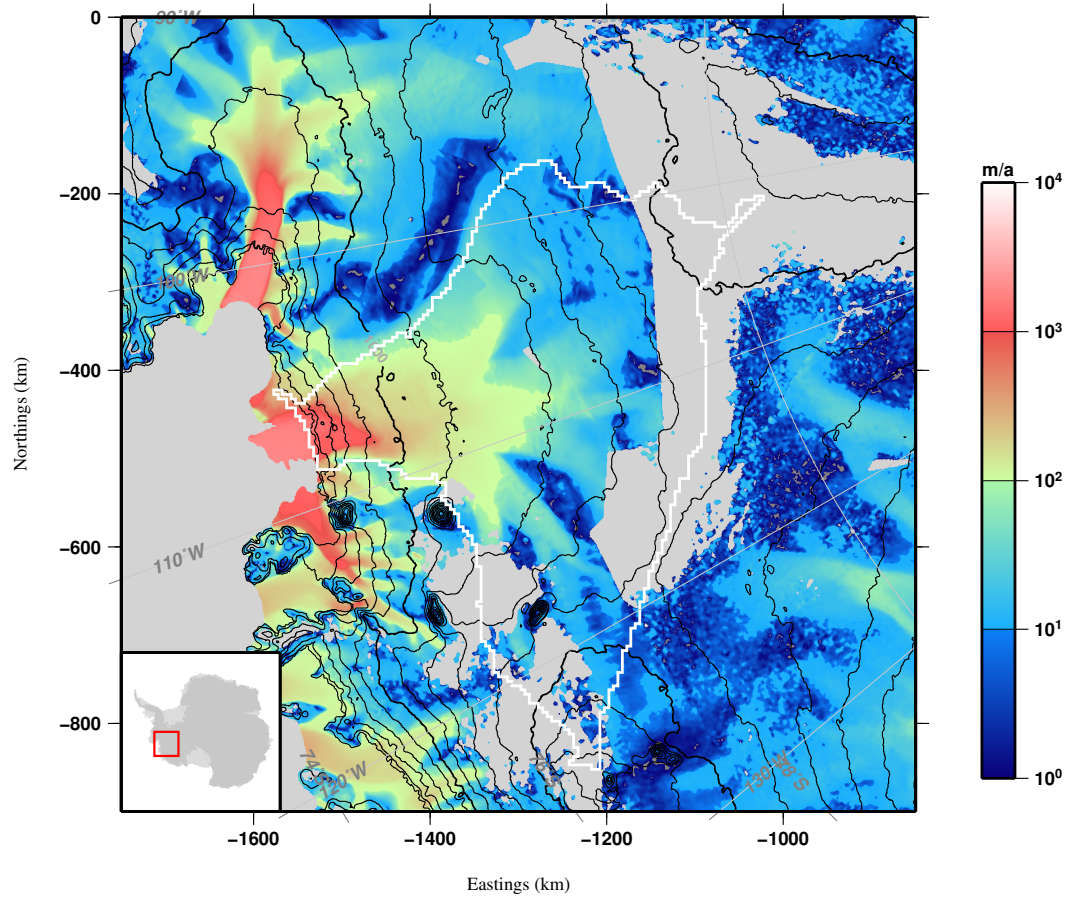


Figure 4.1: InSAR surface velocities [Rignot et al., 2011]

and Paterson [1994], stress can be expressed as a function of these parameters in the equation:

$$\frac{\sigma_{ij}}{dx_j} + \rho g_i = 0 \quad (4.1)$$

where  $i, j = (1, 2, 3)$ ,  $\sigma$  is the stress,  $\rho$  is the ice density, and  $g$  is the force of gravity. Strain rate is a function of the velocity gradient:

$$\dot{\epsilon} = \frac{1}{2} \left[ \frac{du_i}{dx_j} + \frac{du_j}{dx_i} \right] \quad (4.2)$$

with  $\dot{\epsilon}$  corresponding to the strain rate and  $u_i$  to the three-dimensional velocity components.

Assuming the ice is unaffected by hydrostatic pressure and assuming isotropy of the ice [Nye, 1958] in Equations 4.1 and 4.2, the dependence of strain rate on ice velocity can be represented by a cartesian curvilinear system where the vertical plane of a flow line corresponds to the x-z profile and the y-axis to the transverse coordinate (Figure 4.2). Under such a system, the strain rates can be represented as [Reeh, 1988]:

$$\dot{\epsilon}_x = \frac{du}{dx} + \frac{v}{r}, \quad \dot{\epsilon}_y = \frac{dv}{dy} + \frac{u}{R}, \quad \dot{\epsilon}_z = \frac{dw}{dz} \quad (4.3)$$

where  $(u, v, w)$  correspond to the velocity components in the  $(x, y, z)$  directions and  $r$  and  $R$  are the radii of curvature for a flow line and a surface elevation contour, respectively. By convention, negative and positive  $R$  represent divergence and convergence, respectively. We assume the transverse component of velocity,

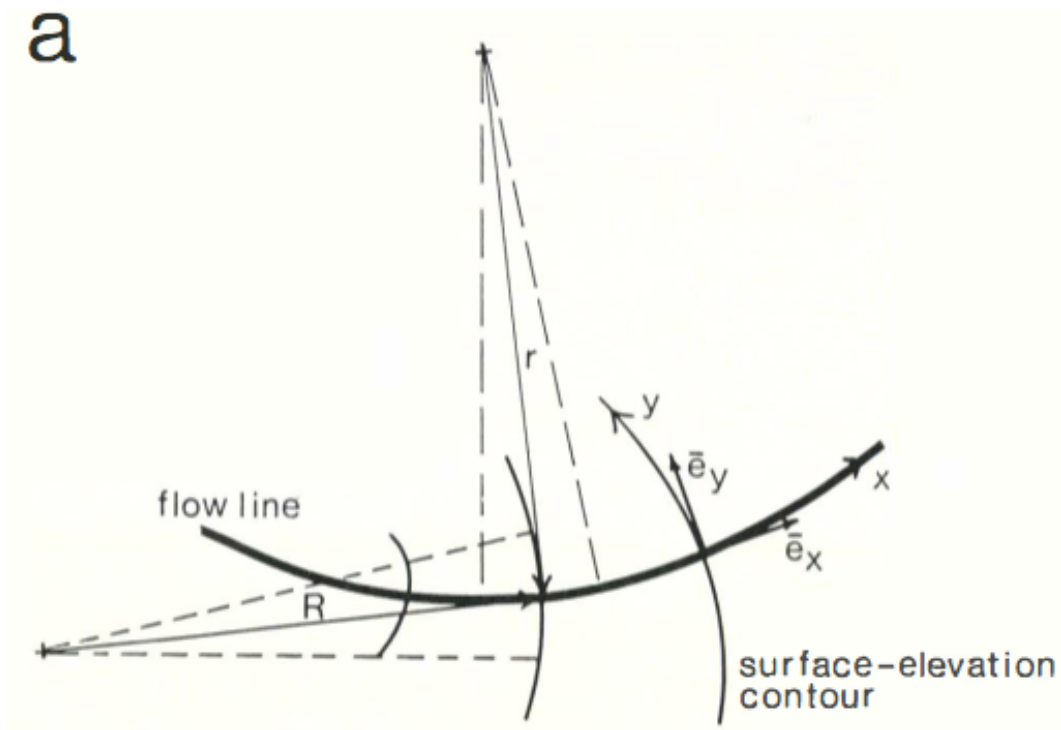


Figure 4.2: Coordinate axis along a flow line [Reeh, 1988], Figure 1a.

$v$ , is zero along a flow line. Furthermore, the condition of mass conservation and incompressibility of ice implies that:

$$\frac{du}{dx} + \frac{u}{R} + \frac{dw}{dz} = 0 \quad (4.4)$$

Ice flux,  $q$ , can be expressed as:

$$q = \int_B^S u dz \quad (4.5)$$

where  $S$  and  $B$  represent the surface and bedrock profiles respectively. Substitution of Equation 4.5 into Equation 4.4 reduces to:

$$\frac{dq}{dx} + \frac{q}{R} = a + b + \frac{dS}{dt} \quad (4.6)$$

with  $a$  as accumulation rate and  $b$  as subglacial melting. Under the condition of (local) steady state where the vertical variation of the surface,  $S$ , with respect to time is equal to zero (i.e., time independent) and there is no melt at the bedrock, Equation 4.6 further simplifies to:

$$\frac{dq}{dx} + \frac{q}{R} = a \quad (4.7)$$

where  $dq/dx$  is specified for the whole ice column. Due to the high degree of uncertainty in ice deformation at the base of TG, the direct application of Equation 4.7 would make accumulation results more uncertain. A first-order estimate is to assume  $dq/dx$  is equal to the accumulation rate calculated using Nye's method

[Leuro et al., in review]. These accumulations are computed based on the age and depth of our layers where there is little layer deformation, permitting us to assume a constant vertical strain rate throughout the ice column. We keep the term  $q/R$  in Equation 4.7 to preserve the influence of glacier geometry (i.e. convergence and divergence) and ice flux. To improve our estimate of accumulation, instead of considering 2-dimensional flow (as in Equation 4.7), I consider ice flux through a flow band oriented along flow. Following the notation from Parrenin et al. [2004], the divergence/convergence of ice within this square cylinder is described by:

$$divergence = \frac{h}{Y} \frac{\partial Y}{\partial x} \bar{U}_x \quad (4.8)$$

where  $h$  is the thickness of the layer,  $Y$  is the transverse width of the flow line,  $x$  is distance along the flow line, and  $\bar{U}_x$  represents the depth-averaged velocity, approximated to be equal to the surface InSAR velocity. The latter is a reasonable assumption for shallow layers.

### 4.3 Computation Of Flow Lines

To calculate the components of Reeh's method (Equation 4.7), I compute 5-km resolution flow lines from balance velocities [Le Brocq et al., 2006], assuming flow is perpendicular to iso-topographic lines. This assumption is not ideal given TG is not in steady state [Rignot et al., 2003], but Reeh [1988] point out that the assumption of steady state flow for shallow layers is acceptable. For each flow line, I extract InSAR surface velocities [Rignot et al., 2011], GLAS surface topography

[DiMarzio et al., 2003], and layer depth [Leuro et al., in review]. In order to account for the effects of longitudinal stresses which may introduce noise into the accumulation rate [Le Brocq et al., 2006], I smooth these grids with a 3-point Gaussian filter with width 10 times the layer depth and apply a spatial anti-aliasing filter to remove sampling and interpolation artifacts in the data. We validate our flow line results with those computed by Conway et al. [2010] for flow lines in central TG dating at least 600 years (Figure 4.3).

#### **4.4 Sources Of Error**

The systematic sources of error in our estimates of accumulation rate are a function of the precision of radar travel time measurements, InSAR velocity measurements, ice surface elevations, and the assumption of steady state in TG. The first was described in Peters et al. [2007] and Leuro et al. [in review] and indicates layers resolved to within  $\pm 8.6$  meters. InSAR velocities are measured along the line of sight of the satellite antenna and not necessarily perpendicular to the ground, meaning these velocities are not exactly horizontal and therefore do not equal balance velocities as assumed in Equations 4.5 and 4.7. Inherent InSAR velocity errors (due to atmospheric effects, residual topography, etc.) are smaller than 10 percent [Rignot et al., 2011].

According to Reeh [1988], the assumption of mass balance is valid for at least the upper 10 percent of the ice column. We therefore do not consider our layers to be affected by the non-steady state condition of TG, though this error affects our computations of flow lines nonetheless. For simplicity, I exclude thermal effects,

# Flowlines in Thwaites

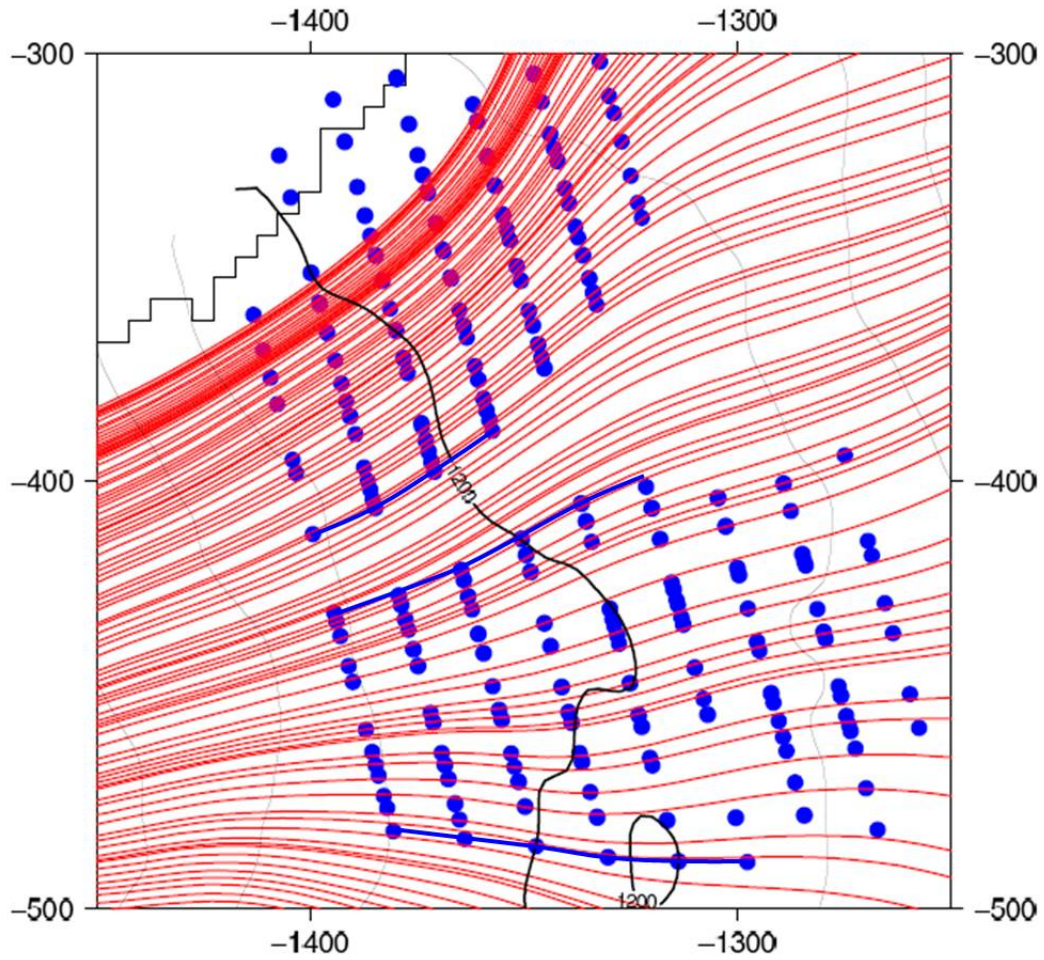


Figure 4.3: Comparison between our flow lines (red lines) and layer flow lines picks identified in englacial structures (green dots) and confirmed by modern GPS [Conway et al., 2010], both showing approximate agreement.



such as ice deformation, that can speed up surface velocities. Other geophysical sources of error, including surface advection and longitudinal strain rates, are not significant and were not included. Basal melting is observed in the catchment of TG, [Schroeder et al., in review]; however, I prefer to exercise caution on including basal melting as a correction for accumulation as I do not see an immediate correlation between bedrock specularity reported by Schroeder et al. [2013] demonstrating basal meltwater and zones of high, localized anomalies of accumulation I observe along flow lines.

## **4.5 Interpretation of Results**

The result of Equation 4.7 for estimating accumulation rate is shown in Figures 4.4 and 4.5, for layers 1 and 2, respectively. The most significant feature at the TG scale is decreasing accumulation rates from the coastal area to the ice divide, with accumulation rates ranging from more than 3.0 m/yr to less than 0.1m/yr. The accumulation rate decay is a consequence of an adiabatic process in which the temperature and atmospheric pressure of a parcel of air decreases as it rises, draining its moisture content via precipitation. This pattern of precipitation corresponds to the general snowfall distribution for large ice sheets [Paterson, 1994]. Local anomalies from this pattern are indicative of the influence of temporal or spatial forcings that can provide indirect information about climate and ice dynamics (e.g. Spikes et al. [2004]).

Over TG, the distribution of accumulation rate deviates from the above described pattern at the location of bedrock topographic tributaries described by Holt

## Layer 1 (Nye+convergence)

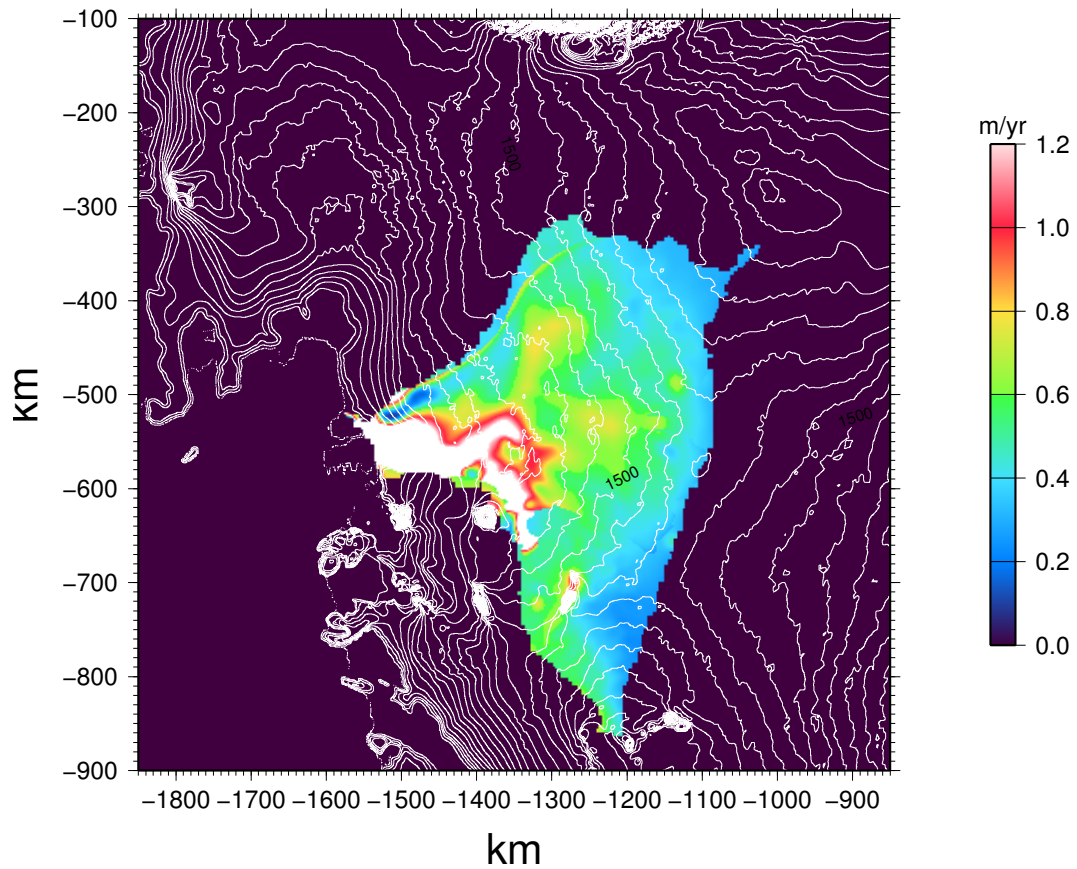


Figure 4.4: Blending of accumulations rates from Nye and Reeh for Layer 1. Mount Takahe is at -1400E, -580N

## Layer 2 (Nye+convergence)

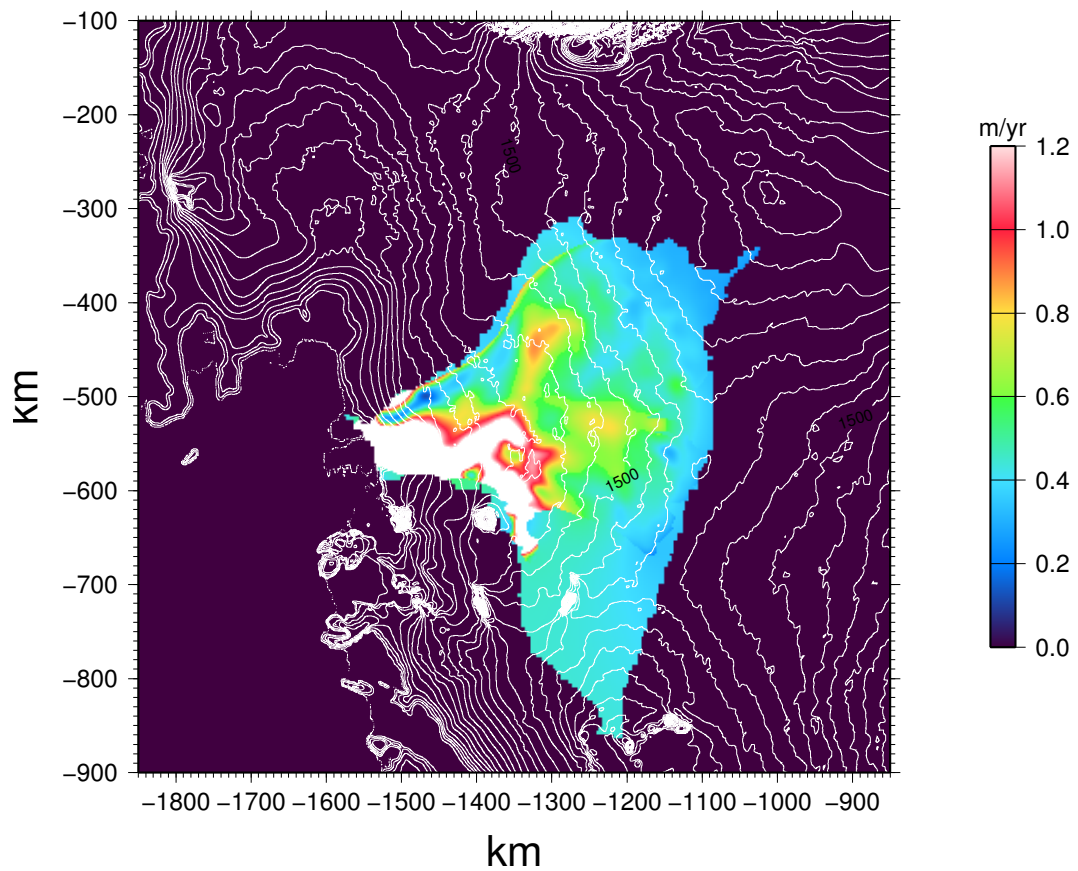


Figure 4.5: Blending of accumulations rates from Nye and Reeh for Layer 2. Mount Takahe is at -1400E, -580N

et al. [2006] (Figure 2.2). This dendritic pattern in accumulation rate is a direct consequence of Equations 4.5 and 4.7, where accumulations are a function of the geometric distribution of ice fluxes and other factors playing a minor, but potentially non-negligible, role such as wind patterns, local topography, and the ice flow regime itself.

Several other significant accumulation rate anomalies are also observed. Near Mount Takahe (longitude -1400E, latitude -500N); Figure 4.1), high and low accumulation anomalies may demonstrate (on a small scale) the aforementioned adiabatic lapse rate effect. Between the limits of Pine Island Glacier and TG, close to the coast, there is a zone of unusually low accumulation values that are also seen in RACMO2 (Figures 4.1,4.4, and 4.5). This anomalously low accumulation is the product of eolian effects at the margin between the two glaciers.

#### **4.6 Comparison with RACMO2.1 and AMSR Inferences of Accumulation**

We further test our accumulation results by comparing them with RACMO2.1 [Lenaerts et al., 2012b] and an interpolation based on AMSR data [Arthern et al., 2006] that infers accumulation rates based on the ratio of vertical and horizontal polarization of thermal radiation in a layered density profile, combined with in situ measurements. Figure 4.6 shows average accumulation rates binned every 50 meters of altitude for the entire TG catchment. We observe that both AMSR and Nye (before divergence) agree to first-order along the coast and toward the interior. At low elevations, both approaches have improbably low accumulation values when

compared to RACMO2.1. In general, AMSR underestimate accumulations when compared to RACMO so the overlap with our Nye results is coincident.

RACMO2.1, as demonstrated by the snow radar measurements of Medley et al. [2013], is valid for altitudes between 1000 m and 1800 m above sea level, but underestimates accumulations above this altitude (see Figure 4.6). If the steady state assumption were valid for TG, the addition of Nye and the divergence correction (Equation 4.8) should account for the apparent deficit in accumulation rate calculated from radar measurements. Instead, our results show an anomalously high accumulation rate below 1300 m, where the application of divergence overshoots RACMO2.1.

The discrepancy between Nye-plus-divergence and RACMO2.1 is likely too high to be created by the atmosphere, even if a climate disturbance was sustained for thousands of years. Therefore, our resulting submergence velocities are inconsistent with realistic values of snowfall. The steady state assumption inherent in these models is likely incorrect up to 200 km inland of the grounding line of TG, (1500 m elevation) where surface velocities start to increase rapidly above, 1.5km/yr. There are two possible scenarios that would explain this discrepancy: velocities in the past were slower or the surface topography previously had a different configuration, a situation that would imply different flow line patterns in the past. Both explanations are consistent with a decreasing buttressing effect from the TG ice tongue about a century in the past [Tinto and Bell, 2011].

We rule out the second hypothesis for central TG because our computed flow lines are similar to independently computed flow lines at least 600 years old

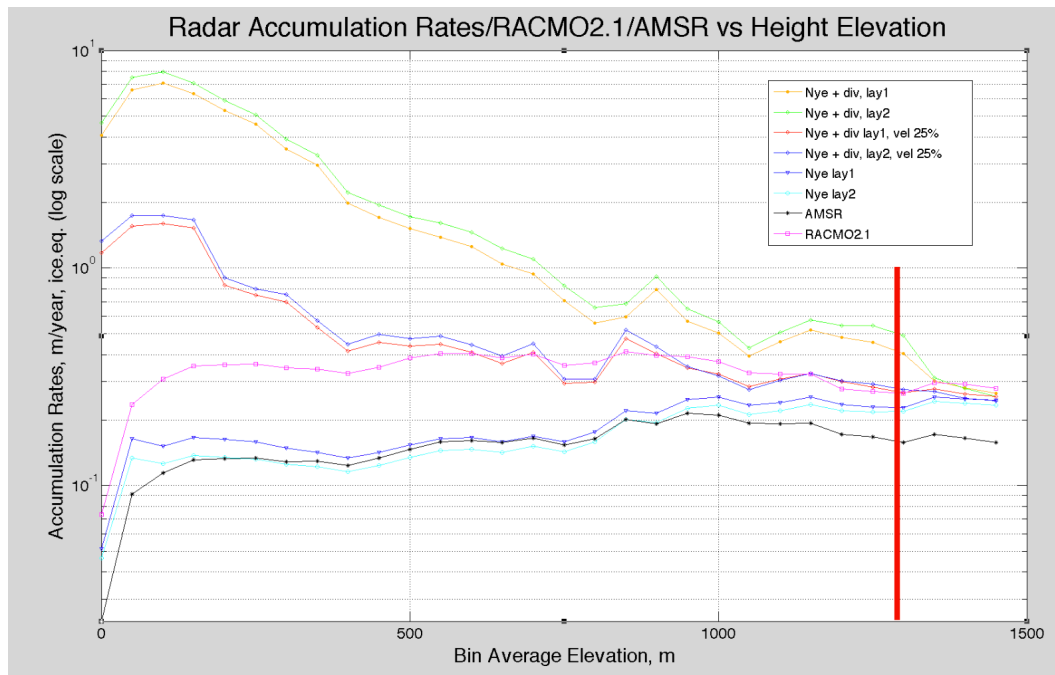


Figure 4.6: Comparison of different accumulation rates models as a function of elevation, including the InSAR velocity reduced to 75% that matches RACMO. AMSR is the Arthern et al. [2006] interpolation. Red vertical line represents  $D=1$

RACMO2.1 (Lenaerts et al., 2012)

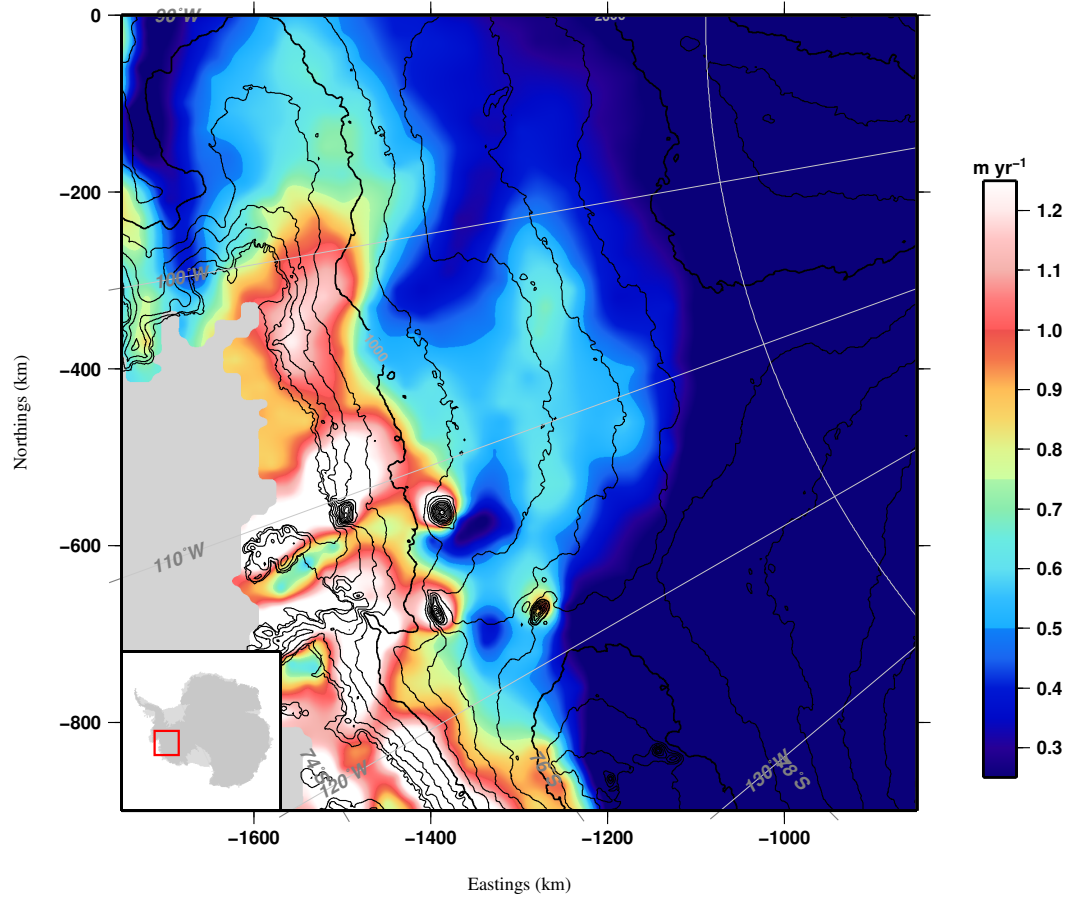


Figure 4.7: The RACMO2.1 atmospheric model of surface mass balance [Lenaerts and van den Broeke, 2012]

(Figure 4.3; Conway et al. [2010]). This suggests that ice flow has not changed significantly since layer 1 was deposited. Because the divergence and convergence of layer 1 and 2 are similar (Figures 4.4 and 4.5), I infer that the flow direction of layer 2 has similarly not experienced a significant change. As discussed previously, I do not have evidence to extend this conclusion to areas near the coast. However, if I assume flowlines behave similarly in areas of fast and slow ice flow, I can assume there has been an increase in ice velocities that began after deposition of the layers.

I now determine the velocity adjustment needed to match my results with RACMO2.1. To do this, I apply a zero-order velocity correction by linearly scaling the contemporary InSAR velocities by a constant. I find that a 75% reduction in InSAR velocity matches RACMO2.1 from 500 m to 1350 m above sea level, and  $D=1$  (see Figure 4.6) that effectively shows the altitude below which the Nye method starts to fail. The reduced velocity required to match our model to RACMO2.1 suggests a significantly slower ice flow in at least the last 700 hundred years than suggested by our radar observations. The reason for this reduction in speed is an open question. Possible causes could be drier basal conditions in the past, or rapid changes in grounding line retreat among others which would lead to the reduced in speed.

## **4.7 Conclusions**

The present results show a comprehensive analysis of accumulation rate for the TG catchment, which includes merging two complementary methodologies: Nye [1958] and Reeh [1988]. The former is valid for areas of low velocity and



small longitudinal gradients, while the later is more appropriate for areas of high velocity and more realistically represents the dependence of snowfall distribution on subglacial topography, as described by [Holt et al., 2006]. We observe the expected trend of decreasing accumulation rate toward the interior of TG. Minor anomalies are observed inland of Mount Takahe as well as some localized high anomalies above 1 m/yr, which might be indicative of basal melting, though I do not see an immediate correlation with the bedrock specularly reported by Schroeder et al. [2013] suggesting the presence of water at the ice-bed interface. We observe a low anomaly in the northeast section of TG close to the glacier tongue and at the limits with Pine Island Glacier, which could be related to subregional climate effects as it is also visible in RACMO2.1 (Figure 4.7). From the comparison between RACMO2.1 and our results, I notice our accumulation rates are significantly higher below 1300 m elevation (Figure 4.6), particularly affecting the 200 km upstream of the grounding line. We assert that due to the long-term consistency of flow line patterns, apparent divergence corrected accumulation rate anomalies in this area can be attributed to an increase in ice velocity, rather than changes in accumulation rate over the past 700 years, this increase in velocity is approximately equal to 75%, the reason for its causes it's an open question, a possible explanation are a drier basal conditions in the past, or retreat of the grounding line, among others.

## **Chapter 5**

# **Long Term Mass Balance Of Thwaites Glacier, West Antarctica**

### **5.1 Introduction**

Mass balance is defined as the difference between net input mass from snow fall and ice discharge along the grounding line. For Thwaites Glacier (TG), the current input mass in the grounded catchment is significantly lower than ice discharge (See Table 5.1). The rate of input mass can be estimated by interpolating locally determined surface mass balance rates from ice cores, climate, or englacial layer deformation models; however, all of these methods are compromised when assessed at longer time intervals. Ice cores are not deep enough to extend more than a couple hundred years in TG and are usually sparse. Climate models become increasingly unconstrained with time due to increasingly uncertain boundary conditions. In particular, in regions of accelerating ice flow, strong convergence, or strong gradients in ice depth and accumulation rate become increasingly difficult to model [Waddington et al., 2007]. Here, using two well-dated layers collected on a survey of the entire TG catchment, I instead estimate total mass balance by evaluating the volume of input ice over the age of the layer. We then assess scenarios for ice loss over the grounding line to estimate TG's mass balance since our layers were deposited. Finally, I compare our results with modern estimates of mass balance and how our

spatial and temporal coverage allows us to get more comprehensive results.

## **5.2 Area Description**

TG is the second largest glacier of the West Antarctic Ice Sheet (WAIS), draining an area of approximately 165,000 km<sup>2</sup>. It drains into the Amundsen Sea, to the east of Pine Island Glacier (PIG), and is flanked to the west by Marie Byrd Land. TG is a marine ice sheet with its ice-bedrock interface well below sea level and surface elevations higher than 2000 m above sea level. It is unrestrained by a significant ice shelf. Satellite observations of the last 20 years show grounding line retreat along with acceleration and thinning of the ice column in the sector of fast flow close to the coast [Rignot et al., 2004]. TG catchment is underlain by a single deep basin bounded by a broad coastal sill of low topographic relief, and is fed by a dendritic pattern of deeply incised valleys [Holt et al., 2006]. All six of the TG tributaries identified by Rignot et al. [2011] from ice surface velocities correspond to deep subglacial troughs that control the behavior of surface velocities.

## **5.3 Data**

We use radio echo sounding measurements performed by the University of Texas Institute for Geophysics (UTIG) from 2004/05 over the catchment of TG, West Antarctica to track ice depth. The survey covers the catchment with a 15 x 15 km grid of profiles, aligned with the coast. We use the High Capability Airborne Radar Sounder (HiCARS, Peters et al. [2005]) with 60 MHz center frequency, 15 MHz bandwidth and a 100 ns compressed pulse width. To estimate

the ice-equivalent depth of internal reflectors, I use a constant two way velocity of  $169\text{m}\mu\text{sec}^{-1}$ , yielding a bandwidth resolution equivalent to 8.5 m. We track two shallow, continuous layers (layer 1 and layer 2) present over the majority of the ice catchment. These layers range in depth from  $\sim 80$  m at ice divide to  $\sim 600$  m in the coastal area, their average depth in the catchment is 243 m and 313 m respectively, and they are assumed to be isochrones throughout the catchment. Both layers are tied to well-dated tropical volcanic eruptions ( $\pm 2$  year) of global impact, with layer 1 linked to a 1460 CE eruption, and layer 2 corresponding to a 1257 CE event [Leuro et al., in review]. These dates yield layer ages of  $548 \pm 20$  yr and  $725 \pm 20$  yr, respectively. A final caveat is that for the AGASEA survey, while continuous layering was observed in most of the inland part of the catchment, in the lower 45 km of the trunk, layers were obscured due to scattering produced by crevassed areas.

## 5.4 Mass Balance Estimations

For estimates of mass balance over TG I use the flux method, defined as the difference between the grounded part of the ice sheet, and the flux discharge across the GL. Numerically, mass balance is equal to [Paterson, 1994]:

$$\text{mass balance} = \text{input} - \text{output} \quad (5.1)$$

The input balance corresponds to the volume of the grounded ice of layers 1 and 2, (Table 5.1). The second term, the output balance, or calving and melting

Table 5.1: Input Mass for TG, adapted from Medley et al. [2013]  $\text{Gt yr}^{-1}$

Source	Citation	Mean, i.e.
IceBridge	Medley et al. [2014]	$75.9 \pm 5.2$
RACMO2.1	Lenaerts et al. [2012b]	$74.6 \pm \text{NR}$
ERA-interim	Dee et al. [2011]	$66.9 \pm \text{NR}$
CSFR	Saha et al. [2010]	$71.8 \pm \text{NR}$
MERRA	Rienecker et al. [2011]	$61.0 \pm \text{NR}$
ART06	Arthern et al. [2006]	$54.5 \pm \text{NR}$
MON06	Monaghan et al. [2006]	$89.0 \pm \text{NR}$
Layer 1	This work	$88.8 \pm 5.9$
Layer 2	This work	$88.6 \pm 7.1$

(to a lesser extent) across the grounding line (GL), is equal to the ice depth at the GL multiplied by the depth-averaged velocity. For our case, I assume the depth-averaged velocity [Rignot et al., 2008] is equal to the average velocity observed from InSAR, a valid approximation at the GL [Paterson, 1994]. We compute the input mass balance in two steps: first, I estimate the volume of each layer, and second, I add the flux discharge across the GL since the time of layer deposition. For the output balance, I use the published results of flux discharge from Mougnot et al. [2014] for 2004, the year of our data collection (Table 5.2).

## 5.5 Ice Volume Retained

The input mass over the catchment has two components: the ice volume still resident (ice retained) in the ice sheet, and the ice volume that has been lost to the ocean since the layer was deposited. To derive the first I use catchment bounds derived from the Bamber and Bindschadler [1997] radar altimetry digital

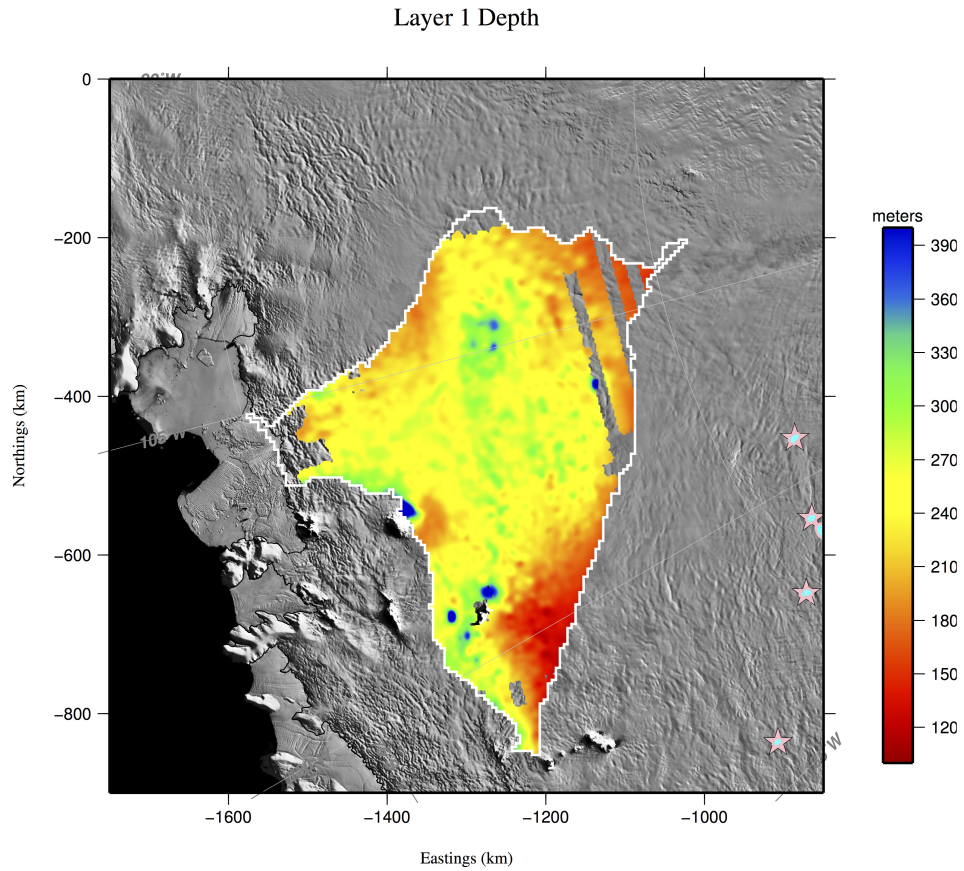


Figure 5.1: Map of the depth to layer 1, using the Thwaites Glacier catchment and lack of data as a mask. The background is the Mosaic of Antarctica (MOA) [Scambos et al., 2007]

elevation model [Vaughan et al., 2001], which provides  $167.6 \times 10^3 \text{ km}^2$ . of area for the catchment of TG. We interpolate the layer depths to a grid resolution of 2.5 km using a bicubic spline, mask the layers to the divide of TG, and determine the volume of ice above each layer. We find volumes of retained ice equal to  $39.5 \times 10^3 \text{ km}^3$  for layer 1 and  $50.9 \times 10^3 \text{ km}^3$  for layer 2 (Figures 5.1 and 5.2).

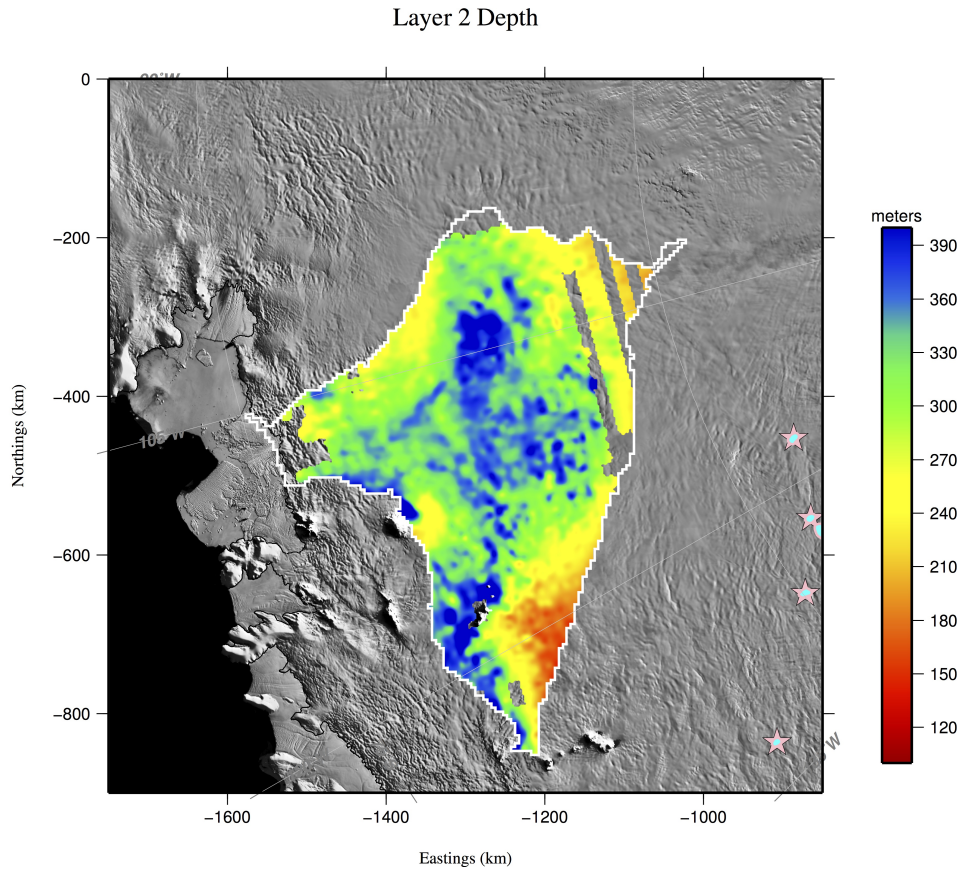


Figure 5.2: Map of the depth to layer 2, using the Thwaites Glacier catchment and lack of data as a mask. The background is the Mosaic of Antarctica (MOA) [Scambos et al., 2007]

### 5.5.1 Sources of error in ice volume retained

Other estimates of the TG area are  $182 \times 10^3 \text{ km}^2$  [Rignot et al., 2008], and  $175.9 \times 10^3 \text{ km}^2$  [Medley et al., 2014], obtained primarily by extending the TG catchment south of an area of low accumulation. These values imply an area uncertainty of  $15 \times 10^3 \text{ km}^2$  (i.e. the difference between Rignot's area and ours). Assuming that the layers are flat in the ice divide area, I estimate an ice volume

uncertainty of  $\pm 2.7 \times 10^3 \text{ km}^3$  and  $\pm 3.5 \times 10^3 \text{ km}^3$ , respectively, due to catchment uncertainty, which will be relatively high due to large area difference between the assumed catchments.

An additional source of uncertainty is due to the resolution of the radar sounder. Interpreted conservatively, this represents a volume uncertainty of

$$8.5\text{m} \times 167.6 \times 10^3 \text{ km}^2 = 1.4 \times 10^3 \text{ km}^3 \quad (5.2)$$

for each layer.

The last source of uncertainty is the unquantified layer depths in the 45 km of fast-flowing ice upstream of the GL that does not have layers that can be tracked reliably due to strong surface crevassing. Occasional gaps in the crevasses show flat-lying layers, implying that the depths of layer 1 and layer 2 do not change significantly; however, I cannot connect the layers, so I rely on the interpolated results from a bicubic spline algorithm [Wessel and Smith, 1998]. We interpolate volumes of  $0.9$  and  $1.2 \times 10^3 \text{ km}^3$  for layer 1 and layer 2 in this region.

A limiting scenario for the error in the retained volume assumes vertical advection of the layers toward the bottom of the ice sheet in the data gap upstream of the GL. In this case, the total volume of ice in the layer data gap near the GL generated by the vertical advection is approximately to  $4.4 \times 10^3 \text{ km}^3$ . Therefore, including the entire ice volume in the data gap, I get an additional ice volume uncertainty beyond our interpolation of  $3.5$  and  $3.2 \times 10^3 \text{ km}^3$  for each respective layer. For layer 1 the maximum uncertainty in retained ice volume is



$$(0 \text{ to } +3.5) \times 10^3 + (0 \text{ to } 2.7) \times 10^3 \pm 1.4 \times 10^3 = -1.4 \text{ to } +7.6 \times 10^3 \text{ km}^3 \quad (5.3)$$

and for layer 2

$$(0 \text{ to } +3.2) \times 10^3 + (0 \text{ to } 3.5) \times 10^3 \pm 1.4 \times 10^3 = -1.4 \text{ to } +8.1 \times 10^3 \text{ km}^3 \quad (5.4)$$

Therefore, our estimated volume of ice retained for layer 1 is  $37.7 \times 10^3$  to  $46.7 \times 10^3 \text{ km}^3$  and for layer 2 is  $49.5 \times 10^3$  to  $58.1 \times 10^3 \text{ km}^3$ . Ice input fluxes, considering only the volumes of ice retained, are conservatively  $69.1$  to  $85.6 \text{ km}^3 \text{ yr}^{-1}$  for layer 1 and  $66.1$  to  $77.7 \text{ km}^3 \text{ yr}^{-1}$  layer 2.

## 5.6 Ice Volume Lost

Over the age of each layer, a portion of the ice volume is lost over the grounding line. As the layers used are here within the non-shearing upper part of the ice column, I can estimate the volume of ice lost as the flux through a gate represented by the vertical area of the layer at the grounding line. This volume can be thought of as a wedge of ice advected past the grounding line at the ice velocity, the bottom surface of which is the depth of the layer and the upper surface is ice that has just been deposited and has not yet moved significantly (Figure 5.3). For ice that is not shearing, this concept can be expressed as

$$V_{lay} = V_r + \frac{(\overline{UYT}_{lay} h_{lay})}{2} \quad (5.5)$$

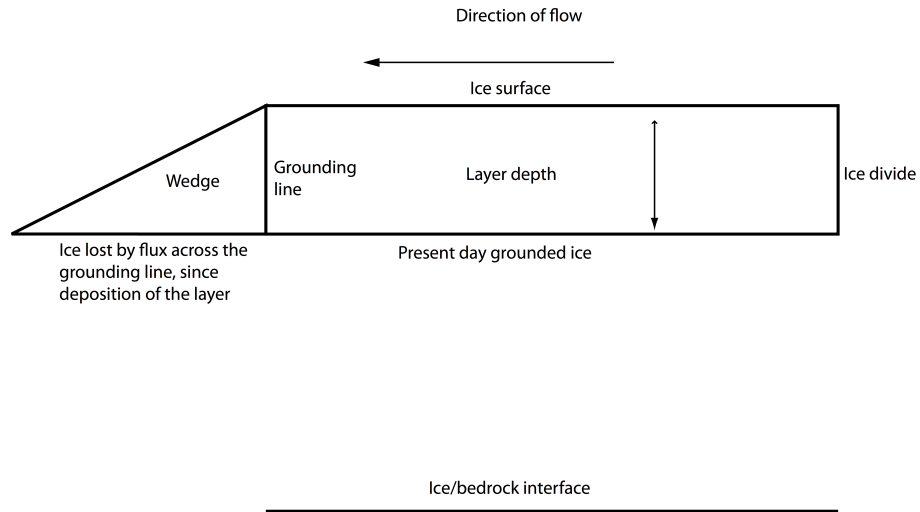


Figure 5.3: Diagram of the concepts of the total ice volume deposited, retained and lost.

where  $V_{lay}$  is the total volume of the ice that has accumulated since the layer was deposited,  $V_r$  is the ice retained above the layer (estimated in Section 5.5),  $\bar{U}$  is the average ice velocity (in the direction of the GL from the ice divide) at the grounding line,  $Y$  is the width of the grounding line,  $T_{lay}$  is the age of the layer, and  $h_{lay}$  is the depth of the layer at the grounding line. The biggest uncertainties are in  $\bar{U}$  and  $h_{lay}$ . We initially assume that the average  $\bar{U}$  is the same as the surface velocity observed by InSAR in 2007 [Rignot et al., 2011]. For each layer, I estimate  $h_{lay}$  in the layer data gap in three ways: a) the layer depth in the gap is equal to the depth of the ice sheet at the grounding line; b) the layer depth in the gap is a result of a linear interpolation from the observed layer depth to the base of the grounding line; and c) the layer depth in the gap is scaled proportionally to the ice sheet depth between the survey and the grounding line. Our results are shown in Table 5.2.

Table 5.2: Ice lost over the grounding line ( $\text{km}^3$ ) and implied total input fluxes ( $\text{km}^3\text{yr}^{-1}$ )

Case	layer 1 volume lost	layer 2 volume lost	Input flux 1	Input flux 2
Full depth	$40.4 \times 10^3$	$55.5 \times 10^3$	116.4 to 125.4	126.5 to 136.0
Interpolated contemporary	$11.1 \times 10^3$	$20.4 \times 10^3$	92.3	98.3
Interpolated paleo-velocity	$2.8 \times 10^3$	$5.1 \times 10^3$	77.2	77.2

## 5.7 Discussion of Results

Our input mass balance values are higher than those from other independent estimates (Table 5.3), however, our layers have the advantage of covering the entire catchment with a radar vertical resolution of 8.65 m, which implies a layer age resolution of  $\pm 20\text{yr}$  and an empirically determined age precision of  $\pm 2\text{yr}$  [Leuro et al., in review]. Our estimates are in close agreement with those from Medley et al. [2013], who uses high resolution snow radar to derive the most reliable measure of accumulation rates in TG to present. The only caveat is that Medley et al. [2013] provide estimates over the entire catchment that are based on an extrapolated input balance obtained from a Kriging interpolation, which gives reasonable values for the expected range of accumulation, but is not constrained by ice flow kinematics.

Present day observations show changes of  $dS/dt$  (where  $S$  is surface elevation) and surface velocity,  $v$ , [Rignot et al., 2003] over WAIS at the decadal scale, which is restricted to a time series of 40 years (the beginning of satellite measurements), introducing a bias to the interpretation. An advantage of our approach is that our layers are sufficiently old to allow the decadal variations of velocity and surface elevation to average out, while ensuring the preservation of centennial trends (or the lack of these).

Table 5.3: Mass Balance of TG ( $\text{Gt yr}^{-1}$ ), adapted from Medley et al. [2014] and Mouginit et al. [2014]

Source	Time Period	Input	output	Mass Balance
Mouginit et al. [2014]	1992-2006	-	-107 $\pm$ 4	-
Medley et al. [2014]	1985-2009	76 $\pm$ 5	-	-
Medley et al. [2014]	1994-2010	-	-106 $\pm$ 3	-30 $\pm$ 6
Shepherd et al. [2012]	1992-2011	-	-	-13 $\pm$ 5
Radar (Layer 1) present day velocity (2004)	1459-2004	84.63	-101.4	-11.2 $\pm$ 6.2
Radar (Layer 2) present day velocity (2004)	1257-2004	90.14	-101.4	-11.0 $\pm$ 6.2
Radar (Layer 1) past velocity 25% of present (2004)	1459-2004	70.78	-25.4	45.4 $\pm$ 6.2
Radar (Layer 2) past velocity 25% of present (2004)	1257-2004	70.79	-25.4	45.4 $\pm$ 6.2

## 5.8 Conclusions

Our results show that TG has a mass balance of -11 Gt/yr. A value smaller than previous estimates. We have confidence in our results from the point of view that our layers cover the whole catchment and better capture the details of ice kinematics, thanks to a high radar vertical resolution of 8.65 m. Our results are also in close agreement with the Medley et al. [2014] validation of RACMO2.1 in central TG and with the results from Leuro et al. [in review]. In addition, the age of our layers allows us to see the integrated effect of mass balance in the last 700 years, capturing (possible) long term trends, and averaging out the present day short term fluctuations in snow accumulation that bias contemporary satellite based observations.

The observation that our ice flux discharge at the grounding line is smaller than that of Medley et al. [2014], Mouginit et al. [2014] and Shepherd et al. [2012] is indicative of either larger accumulation rates in the past or an increase in ice velocity [Rignot et al., 2008]. We favor the second hypothesis, as the data also show Leuro et al. [in review] that accumulation rates have remained constant in the last 700 years. The suggested increase in velocities for TG indicate that, sometime since the time of deposition of our layers, TG has undergone one or more changes in dy-

dynamic state as indicated by Tinto and Bell [2011]. However, the four-fold increase in velocity indicated by matching layer thickness to the RACMO atmospheric predictions in chapter 4 are too high as shown by the significantly positive balances presented in table 5.3.

## **Chapter 6**

### **Summary/Conclusions**

An important concept in glaciological studies is the one of mass balance, which is defined as the difference between input mass, in the form of snow fall, and the output mass, such as calving of glaciers. Glaciers are unlikely to be in steady state due to seasonal variations in climate, for example seasonal extremes in accumulation (high and low) during winter and summer, which can vary up to 30% [Neumann et al., 2008]. Spatial variations of mass balance come mainly from the geometrical configuration of the glacier surface. This configuration changes in response to external forcing, including variations in the position of the grounding line as a result of ocean-induced temperature changes. Two glaciers at the same geographical location with different geometrical configurations may respond and readjust differently to the same stimuli.

The focus of this work is Thwaites Glacier (TG), one of the two largest glaciers in West Antarctica, the other being Pine Island Glacier. TG and Pine Island are two of the largest Antarctic contributors to global sea level rise due to their larger than average flux discharges. Snow fall on these glaciers is currently not enough to balance ice flux into the ocean, resulting in overall ice mass loss [Shepherd et al., 2012]. The goal of this dissertation is to understand the mass balance of TG on

longer timescales than previous work, using a data set that has dense coverage of the entire TG catchment.

In Chapter 3, I use the local layer approximation alone to estimate accumulation rates. This analysis includes the dating of two key englacial layers, verified with reported historical volcanic eruptions. Our derived accumulation rates are lower than those of RACMO2.1 below 1300 m above sea level at the location where the "D" parameter of Waddington et al. [2007] predicts that the assumptions of Nye's accumulation rate fails due to excessive ice deformation. Nonetheless, our results are consistent with those of Medley et al. [2013], which is the most reliable modern estimate of snow fall.

Chapter 4 attempts to correct for the effects of ice flow and surface geometry, assuming steady state dynamics. We apply a divergence correction derived from surface topography and confirmed by englacial structure, and demonstrate that accumulation rates are strongly dependent on surface configuration. We validate our ice flow lines with the flow lines from Conway et al. [2010]; the agreement between the two implies that the convergence pattern has not changed since the deposition of the layers. Large anomalies in accumulation rate are observed in the 200 km upstream of the grounding line, suggesting velocities were slower at the time of deposition of the layers analyzed in this study as first proposed by Rignot et al. [2011]. Our results from Chapter 4 include steady state kinematics and have a more extensive coverage over the TG catchment than Medley et al. [2014]; however, large apparent accumulation rate anomalies imply that TG is not in steady state.

In the absence of steady state conditions, inferring mass balance from kine-

matic inference of accumulation rates is complex. Therefore in Chapter 5, I use our extensive coverage of the TG catchment for a different approach: directly estimating the volume of deposited ice. Our mass balance estimation includes the following caveats. First, I assume the positions of both the grounding line and ice divide have remained constant through time. Second, I lack layer data coverage in the 45 km upstream of the TG grounding line, for which I rely on software interpolation. However, I find that TG has a less negative mass balance over the last half millennium than contemporary estimates.

In summary, I present the most comprehensive model of accumulation rates for TG that allows us to extend and update estimates of mass balance throughout the TG catchment. In addition, I find that most changes in ice flow dynamics in TG have taken place in the 200 km upstream of the grounding line.

This work gives a more solid foundation for constraining models of ice divide migration, grounding line migration, ice flow, ice-ocean-atmosphere interaction, ice tongue buttressing, sea level rise, and ice core analysis, all of which require knowledge of the mass balance.



## Bibliography

- Robert J. Arthern, Dale P. Winebrenner, and David G. Vaughan. Antarctic snow accumulation mapped using polarization of 4.3-cm wavelength microwave emission. *Journal of Geophysical Research*, 111(D6):D06108, March 2006. doi: 10.1029/2004JD005667. URL <http://dx.doi.org/10.1029/2004JD005667>.
- J. L. Bamber and R. A. Bindschadler. An improved elevation dataset for climate and ice-sheet modelling: validation with satellite imagery. *Annals of Glaciology*, 25:438–444, 1997.
- John C. Behrendt. The aeromagnetic method as a tool to identify Cenozoic magmatism in the West Antarctic Rift System beneath the West Antarctic Ice Sheet — A review; Thiel subglacial volcano as possible source of the ash layer in the {WAISCOPE}. *Tectonophysics*, 585(0):124 – 136, 2013. ISSN 0040-1951. doi: 10.1016/j.tecto.2012.06.035. URL <http://www.sciencedirect.com/science/article/pii/S0040195112003605>.
- Robert Bindschadler. The environment and evolution of the West Antarctic ice sheet: setting the stage. *Philos Transact A Math Phys Eng Sci*, 364:1583–1605, 2006a.
- Robert Bindschadler. Hitting the Ice Sheets Where It Hurts. *Science*, 311:1720–1721 (doi:10.1126/science.1125226), 2006b.

D D Blankenship and Duncan A. Young. AGASEA ice thickness profile data from the Amundsen Sea Embayment, Antarctica. Digital media, National Snow and Ice Data Center, Boulder, Colorado USA, 2012. URL <http://dx.doi.org/10.7265/N5W95730>.

D. D. Blankenship, C. R. Bentley, S. T. Rooney, and R. B. Alley. Seismic measurements reveal a saturated porous layer beneath an active Antarctic ice stream. *Nature*, 322(6074):54–57, 1986. doi: 10.1038/322054a0. URL <http://dx.doi.org/10.1038/322054a0>.

Donald D. Blankenship, Duncan A. Young, Scott D. Kempf, Dustin M. Schroeder, Jamin S. Greenbaum, Martin J. Siegert, and Jason L. Roberts. ICECAP HiCARS 1 L1B geolocated radar records. Digital media, NASA DAAC at the National Snow and Ice Data Center, 2014. URL <http://nsidc.org/data/ir1hl1B>.

David H. Bromwich, Julien P. Nicolas, Andrew J. Monaghan, Matthew A. Lazzara, Linda M. Keller, George A. Weidner, and Aaron B. Wilson. Central West Antarctica among the most rapidly warming regions on earth. *Nature Geosciences*, 6(2):139–145, 02 2013. URL <http://dx.doi.org/10.1038/ngeo1671>.

Sasha P Carter, Donald D. Blankenship, Duncan A. Young, and John W. Holt. Using radar-sounding data to identify the distribution and sources of subglacial water: application to Dome C, East Antarctica. *Journal of Glaciology*, 55(194):1025–1040, 2009. doi: 10.3189/002214309790794931. URL <http://dx.doi.org/10.3189/002214309790794931>.

- Josefino C. Comiso. Variability and trends in Antarctic surface temperatures from in situ and satellite infrared measurements. *Journal of Climate*, 13:1674–1696 (doi:10.1175/1520–0442(2000)013!1674: VATIASO2.0.CO;2), 2000.
- Howard Conway, Ginny A. Catania, and T.J. Fudge. Ice flow history of the Thwaites Glacier, West Antarctica. Digital media, National Snow and Ice Data Center, Boulder, Colorado USA, 2010.
- I. W. D. Dalziel and L. A. Lawver. The lithospheric setting of the West Antarctic Ice Sheet. In R. B. Alley and R. Bindshadler, editors, *The West Antarctic Ice Sheet: Behavior and Environment*, volume 77 of *Antarctic Research Series*, pages 13–44. American Geophysical Union, 2001.
- Ian Dalziel and Lawrence Lawver. The lithospheric setting of the West Antarctic ice sheet. *The West Antarctic ice sheet: behavior and environment. Antarctic Research Series. Washington D.C., American Geophysical Union, AGU, 77:29–44*, 2001.
- W. Dansgaard and S. J. Johnsen. A flow model and a time-scale for the ice core from Camp Century, Greenland. *Journal of Glaciology*, 8(53):215–223, 1969.
- DP Dee, SM Uppala, AJ Simmons, P Berrisford, P Poli, S Kobayashi, U Andrae, MA Balmaseda, G Balsamo, P Bauer, et al. The ERA-Interim reanalysis: Configuration and performance of the data assimilation system. *Quarterly Journal of the Royal Meteorological Society*, 137(656):553–597, 2011.
- J. P. DiMarzio, H. J. Zwally, A. C. Brenner, and T. Sidel. Ice Sheet Surface Topography of Greenland and Antarctic from ICESat Altimetry. *AGU Fall Meeting*

*Abstracts*, pages A420+, 2003. URL [http://adsabs.harvard.edu/cgi-bin/nph-bib\\_query?bibcode=2003AGUFM.C32A0420D&db\\_key=PHY](http://adsabs.harvard.edu/cgi-bin/nph-bib_query?bibcode=2003AGUFM.C32A0420D&db_key=PHY).

Mark Fahnestock, Waleed Abdalati, Ian Joughin, John Brozena, and Prasad Gogineni. High geothermal heat flow, basal melt, and the origin of rapid ice flow in central Greenland. *Science*, 294(5550):2338–2342, 2001. URL <http://www.sciencemag.org/cgi/content/abstract/294/5550/2338>.

P. Fretwell, H. D. Pritchard, D. G. Vaughan, J. L. Bamber, N. E. Barrand, R. Bell, C. Bianchi, R. G. Bingham, D. D. Blankenship, G. Casassa, G. Catania, D. Callens, H. Conway, A. J. Cook, H. F. J. Corr, D. Damaske, V. Damm, F. Ferraccioli, R. Forsberg, S. Fujita, Y. Gim, P. Gogineni, J. A. Griggs, R. C. A. Hindmarsh, P. Holmlund, J. W. Holt, R. W. Jacobel, A. Jenkins, W. Jokat, T. Jordan, E. C. King, J. Kohler, W. Krabill, M. Riger-Kusk, K. A. Langley, G. Leitchenkov, C. Leuschen, B. P. Luyendyk, K. Matsuoka, J. Mouginot, F. O. Nitsche, Y. Nogi, O. A. Nost, S. V. Popov, E. Rignot, D. M. Rippin, A. Rivera, J. Roberts, N. Ross, M. J. Siegert, A. M. Smith, D. Steinhage, M. Studinger, B. Sun, B. K. Tinto, B. C. Welch, D. Wilson, D. A. Young, C. Xiangbin, and A. Zirizzotti. Bedmap2: improved ice bed, surface and thickness datasets for Antarctica. *The Cryosphere*, 7:375–393, 2013. doi: 10.5194/tc-7-375-2013.

R. C. A. Hindmarsh. Ice-stream surface texture, sticky spots, waves and breathers: the coupled flow of ice, till and water. *Journal of Glaciology*, 44:589–614, 1998.

John W. Holt, Donald D. Blankenship, David L. Morse, Duncan A. Young, Matthew E. Peters, Scott D. Kempf, Thomas G. Richter, David G. Vaughan, and

Hugh Corr. New boundary conditions for the West Antarctic ice sheet: Subglacial topography of the Thwaites and Smith Glacier catchments. *Geophysical Research Letters*, 33(L09502), May 2006. doi: 10.1029/2005GL025561. URL <http://dx.doi.org/10.1029/2005GL025561>.

Ian R. Joughin, Slawek M. Tulaczyk, Jonathan L. Bamber, Donald D. Blankenship, John W. Holt, Ted A. Scambos, and David G. Vaughan. Basal conditions for Pine Island and Thwaites Glaciers, West Antarctica, determined using satellite and airborne data. *Journal of Glaciology*, 55(190):245–257, 2009.

Susan Kaspari, Paul A. Mayewski, Daniel A. Dixon, Vandy Blue Spikes, Sharon B. Sneed, Michael J. Handley, and Gordon S. Hamilton. Climate variability in West Antarctica derived from annual accumulation-rate records from ITASE firn/ice cores. *Annals of Glaciology*, 39(1):585–594, 2004. doi: 10.3189/172756404781814447. URL <http://dx.doi.org/10.3189/172756404781814447>.

J.-F. Lamarque, T. C. Bond, V. Eyring, C. Granier, A. Heil, Z. Klimont, D. Lee, C. Lioussé, A. Mieville, B. Owen, M. G. Schultz, D. Shindell, S. J. Smith, E. Stehfest, J. Van Aardenne, O. R. Cooper, M. Kainuma, N. Mahowald, J. R. McConnell, V. Naik, K. Riahi, and D. P. van Vuuren. Historical (1850–2000) gridded anthropogenic and biomass burning emissions of reactive gases and aerosols: methodology and application. *Atmospheric Chemistry and Physics*, 10(15):7017–7039, 2010. doi: 10.5194/acp-10-7017-2010. URL <http://www.atmos-chem-phys.net/10/7017/2010/>.

Oliver Lang, Bernhard T. Rabus, and Stefan W. Dech. Velocity map of the Thwaites Glacier catchment, West Antarctica. *Journal of Glaciology*, 50(168):46–56, January 2004. URL <http://www.ingentaconnect.com/content/igsoc/jog/2004/00000050/00000168/art00005>.

Franck Lavigne, Jean-Philippe Degeai, Jean-Christophe Komorowski, Sébastien Guillet, Vincent Robert, Pierre Lahitte, Clive Oppenheimer, Markus Stoffel, Céline M. Vidal, Surono, Indyo Pratomo, Patrick Wassmer, Irka Hajdas, Danang Sri Hadmoko, and Edouard de Belizal. Source of the great A.D. 1257 mystery eruption unveiled, Samalas volcano, Rinjani Volcanic Complex, Indonesia. *Proceedings of the National Academy of Sciences*, 2013. doi: 10.1073/pnas.1307520110. URL <http://www.pnas.org/content/early/2013/09/26/1307520110.abstract>.

Anne M Le Brocq, Antony J Payne, and Martin J Siegert. West Antarctic balance calculations: Impact of flux-routing algorithm, smoothing algorithm and topography. *Computers & Geosciences*, 32(10):1780–1795, 2006. URL <http://www.sciencedirect.com/science/article/B6V7D-4KCPV8P-1/2/0dc32db5ab60ee56c819e6265f132727>.

Wesley E. LeMasurier. Neogene extension and basin deepening in the West Antarctic rift inferred from comparisons with the East African rift and other analogs. *Geology*, 36(3):247–250, March 2008. doi: 10.1130/G24363A.1. URL <http://dx.doi.org/10.1130/G24363A.1>.

- J. T. M. Lenaerts and M. R. van den Broeke. Modeling drifting snow in Antarctica with a regional climate model: 2. Results. *Journal of Geophysical Research: Atmospheres*, 117(D5):n/a–n/a, 2012. ISSN 2156-2202. doi: 10.1029/2010JD015419. URL <http://dx.doi.org/10.1029/2010JD015419>.
- J. T. M. Lenaerts, M. R. van den Broeke, S. J. Déry, E. van Meijgaard, W. J. van de Berg, Stephen P. Palm, and J. Sanz Rodrigo. Modeling drifting snow in Antarctica with a regional climate model: 1. Methods and model evaluation. *Journal of Geophysical Research: Atmospheres*, 117(D5):n/a–n/a, 2012a. ISSN 2156-2202. doi: 10.1029/2011JD016145. URL <http://dx.doi.org/10.1029/2011JD016145>.
- J. T. M. Lenaerts, M. R. van den Broeke, W. J. van de Berg, E. van Meijgaard, , and P. Kuipers Munneke. A new, high-resolution surface mass balance map of Antarctica (1979–2010) based on regional atmospheric climate modeling. *Geophysical Research Letters*, 39(L04501), 2012b. doi: 10.1029/2011GL050713. URL <http://dx.doi.org/10.1029/2011GL050713>.
- Erick Leuro, Duncan A Young, Gail R. Gutowski, and Donald D. Blankenship. Millennial scale accumulation rates over the catchment of Thwaites Glacier, Antarctica. *Geophysical Research Letters*, in review.
- Amanda C. Lough, Douglas A. Wiens, C. Grace Barcheck, Sridhar Anandkrishnan, Richard C. Aster, Donald D. Blankenship, Audrey D. Huerta, Andrew Nyblade, Duncan A. Young, and Terry J. Wilson. Seismic detection of an active sub-

- glacial magmatic complex in Marie Byrd Land, Antarctica. *Nature Geoscience*, 6:1031–1035, 2013. doi: 10.1038/ngeo1992.
- M. B. Lythe, D. G. Vaughan, and the BEDMAP Consortium. BEDMAP: A new ice thickness and subglacial topographic model of Antarctica. *Journal of Geophysical Research*, 106:11335–11352, 2001. doi: 10.1029/2000JB900449. URL <http://dx.doi.org/10.1029/2000JB900449>.
- Joseph A. MacGregor, Ginny A. Catania, Howard B. Conway, Dustin M. Schroeder, Ian R. Joughin, Duncan A. Young, Scott D. Kempf, and Donald D. Blankenship. Weak bed control of the eastern shear margin of Thwaites Glacier. *Journal of Glaciology*, 59(217):900–912, 2013. doi: 10.3189/2013JoG13J050. URL <http://dx.doi.org/10.3189/2013JoG13J050>.
- B. Medley, I. Joughin, S. B. Das, E. J. Steig, H. Conway, S. Gogineni, A. S. Criscitiello, J. R. McConnell, B. E. Smith, M. R. van den Broeke, J. T. M. Lenaerts, D. H. Bromwich, and J. P. Nicolas. Airborne-radar and ice-core observations of annual snow accumulation over Thwaites Glacier, West Antarctica confirm the spatio-temporal variability of global and regional atmospheric models. *Geophysical Research Letters*, pages n/a–n/a, 2013. ISSN 1944-8007. doi: 10.1002/grl.50706. URL <http://dx.doi.org/10.1002/grl.50706>.
- B. Medley, I. Joughin, B. E. Smith, S. B. Das, E. J. Steig, H. Conway, S. Gogineni, C. Lewis, A. S. Criscitiello, J. R. McConnell, M. R. van den Broeke, J. T. M. Lenaerts, D. H. Bromwich, J. P. Nicolas, and C. Leuschen. Constraining the recent mass balance of Pine Island and Thwaites glaciers, West



- Antarctica with airborne observations of snow accumulation. *The Cryosphere Discussions*, 8(1):953–998, 2014. doi: 10.5194/tcd-8-953-2014. URL <http://www.the-cryosphere-discuss.net/8/953/2014/>.
- A. Monaghan, D. Bromwich, and S. Wang. Recent trends in antarctic snow accumulation from polar mm5 simulations. *Philosophical Transactions of the Royal Society A: Mathematical, Physical and Engineering Sciences*, 364(1844):1683–1708, 2006. URL <http://dx.doi.org/10.1098/rsta.2006.1795>.
- Andrew Monaghan and David Bromwich. Insignificant Change in Antarctic Snowfall Since the International Geophysical Year. *Science*, 313:827–831, 2006.
- D.L. Morse, D.D. Blankenship, E.D. Waddington, and T.A. Neumann. A site for deep ice coring in West Antarctica: Results from aerogeophysical surveys and thermo-kinematic modeling. *Annals of Glaciology*, 35:36–44, 2002.
- J. Mouginot, E. Rignot, and B. Scheuchl. Sustained increase in ice discharge from the Amundsen Sea Embayment, West Antarctica, from 1973 to 2013. *Geophysical Research Letters*, pages n/a–n/a, 2014. ISSN 1944-8007. doi: 10.1002/2013GL059069. URL <http://dx.doi.org/10.1002/2013GL059069>.
- T. Naish, R. Powell, R. Levy, G. Wilson, R. Scherer, F. Talarico, L. Krissek, F. Niessen, M. Pompilio, T. Wilson, L. Carter, R. DeConto, P. Huybers, R. McKay, D. Pollard, J. Ross, D. Winter, P. Barrett, G. Browne, R. Cody, E. Cowan, J. Crampton, G. Dunbar, N. Dunbar, F. Florindo, C. Gebhardt, I. Graham, M. Hannah, D. Hansaraj, D. Harwood, D. Helling, S. Henrys, L. Hinov, G. Kuhn, P. Kyle, A. Laufer, P. Maffioli, D. Magens, K. Mandernack,

- W. McIntosh, C. Millan, R. Morin, C. Ohneiser, T. Paulsen, D. Persico, I. Raine, J. Reed, C. Riesselman, L. Sagnotti, D. Schmitt, C. Sjunneskog, P. Strong, M. Taviani, S. Vogel, T. Wilch, and T. Williams. Obliquity-paced Pliocene West Antarctic ice sheet oscillations. *Nature*, 458(7236):322–328, 03 2009. doi: 10.1038/nature07867. URL <http://dx.doi.org/10.1038/nature07867>.
- Tom. A. Neumann, Howard Conway, Stephen F. Price, Edwin D. Waddington, Ginny A. Catania, and David L. Morse. Holocene accumulation and ice sheet dynamics in central West Antarctica. *Journal of Geophysical Research*, 113 (F02018), 2008. doi: 10.1029/2007JF000764. URL <http://dx.doi.org/10.1029/2007JF000764>.
- J. F. Nye. Surges in glaciers. *Nature*, 181(4621):1450–1451, 05 1958. doi: 10.1038/1811450a0. URL <http://dx.doi.org/10.1038/1811450a0>.
- J. F. Nye. Correction factor for accumulation measured by the thickness of the annual layers in an ice sheet. *Journal of Glaciology*, 4(36):785–788, 1963.
- F. Parrenin, F. Rémy, C. Ritz, M. J. Siebert, and J. Jouzel. New modeling of the Vostok ice flow line and implication for the glaciological chronology of the Vostok ice core. *Journal of Geophysical Research: Atmospheres*, 109 (D20):n/a–n/a, 2004. ISSN 2156-2202. doi: 10.1029/2004JD004561. URL <http://dx.doi.org/10.1029/2004JD004561>.
- W. S. B. Paterson. *The Physics of Glaciers*. Butterworth Heinmann, 3rd edition, 1994.

- Matthew E. Peters, Donald D. Blankenship, and David L. Morse. Analysis techniques for coherent airborne radar sounding: Application to West Antarctic ice streams. *Journal of Geophysical Research*, 110(B06303), 2005. doi: 10.1029/2004JB003222. URL <http://dx.doi.org/10.1029/2004JB003222>.
- Matthew E. Peters, Donald D. Blankenship, Sasha P. Carter, Duncan A. Young, Scott D. Kempf, and John W. Holt. Along-track focusing of airborne radar sounding data from West Antarctica for improving basal reflection analysis and layer detection. *IEEE Transactions on Geoscience and Remote Sensing*, 45(9):2725–2736, September 2007. doi: 10.1109/TGRS.2007.897416. URL <http://dx.doi.org/10.1109/TGRS.2007.897416>.
- H. D. Pritchard, S. R. M. Ligtenberg, H. A. Fricker, D. G. Vaughan, M. R. van den Broeke, and L. Padman. Antarctic ice-sheet loss driven by basal melting of ice shelves. *Nature*, 484(7395):502–505, 04 2012. doi: 10.1038/nature10968. URL <http://dx.doi.org/10.1038/nature10968>.
- Niels Reeh. A flow-line model for calculating the surface profile and the velocity, strain-rate, and stress fields in an ice sheet. *Journal of Glaciology*, 34(116):46–54, 1988.
- Michele M Rienecker, Max J Suarez, Ronald Gelaro, Ricardo Todling, Julio Bacmeister, Emily Liu, Michael G Bosilovich, Siegfried D Schubert, Lawrence Takacs, Gi-Kong Kim, et al. MERRA: NASA’s modern-era retrospective analysis for research and applications. *Journal of Climate*, 24(14), 2011.

- E. Rignot, R.H. Thomas, P. Kanagaratnam, G. Casassa, E. Frederick, S. Gogineni, W. Krabill, A. Rivera, R. Russell, J. Sonntag, R. Swift, and J. Yungel. Improved estimation of the mass balance of the glaciers draining into the Amundsen Sea sector of West Antarctica from the NASA/CECS 2002 campaign. *Annals of Glaciology*, 39:231–237, June 2003. URL <http://www.ingentaconnect.com/content/igsoc/agl/2004/00000039/00000001/art00036>.
- E. Rignot, G. Casassa, P. Gogineni, W. Krabill, A. Rivera, and R. Thomas. Accelerated ice discharge from the Antarctic Peninsula following the collapse of Larsen B ice shelf. *Geophysical Research Letters*, 31(23), 2004. doi: 10.1029/2004GL020697. URL <http://dx.doi.org/10.1029/2004GL020697>.
- Eric Rignot and David Vaughan *et al.* Acceleration of Pine Island and Thwaites Glaciers, West Antarctica. *Annals of Glaciology*, 34:189–194, 2002.
- Eric Rignot and Robert Thomas. Mass Balance of Polar Ice Sheets. *Science*, 297: 1502–1506, 2002.
- Eric Rignot, Jonathan L. Bamber, Michiel R. van den Broeke, Curt Davis, Yonghong Li, Willem Jan van de Berg, and Erik van Meijgaard. Recent Antarctic ice mass loss from radar interferometry and regional climate modelling. *Nature Geoscience*, 1:106–110, 2008. doi: 10.1038/ngeo102. URL <http://dx.doi.org/10.1038/ngeo102>.
- Eric J. Rignot, Jeremie Mouginot, and B. Scheuchl. Ice flow of the Antarctic ice sheet. *Science*, 333(6048):1427–1430, 2011. doi: 10.1126/science.1208336.

Suranjana Saha, Shrinivas Moorthi, Hua-Lu Pan, Xingren Wu, Jiande Wang, Sudhir Nadiga, Patrick Tripp, Robert Kistler, John Woollen, David Behringer, et al. The NCEP climate forecast system reanalysis. *Bulletin of the American Meteorological Society*, 91(8), 2010.

T. A. Scambos, T. M. Haran, M. A. Fahnestock, T. H. Painter, and J. Bohlander. MODIS-based Mosaic of Antarctica (MOA) data sets: Continent-wide surface morphology and snow grain size. *Remote Sensing of Environment*, 111(2-3):242–257, 2007. doi: 10.1016/j.rse.2006.12.020. URL <http://www.sciencedirect.com/science/article/B6V6V-4PJ0C44-3/2/d8c1d2e121afa44af2ddb740c3531992>.

Dustin M. Schroeder, Donald D. Blankenship, and Duncan A. Young. Evidence for a water system transition beneath Thwaites Glacier, West Antarctica. *Proceedings of the National Academy of Sciences*, pages 1–4, 2013. doi: 10.1073/pnas.1302828110. URL <http://www.pnas.org/content/early/2013/07/03/1302828110.abstract>.

Dustin M. Schroeder, Donald D. Blankenship, Duncan A. Young, and Enrica Quartini. Evidence for elevated and spatially variable geothermal flux beneath the West Antarctic Ice Sheet. *Proceedings of the National Academies of Science*, in review.

Andrew Shepherd, Erik R. Ivins, Geruo A, Valentina R. Barletta, Mike J. Bentley, Srinivas Bettadpur, Kate H. Briggs, David H. Bromwich, René Forsberg, Natalia Galin, Martin Horwath, Stan Jacobs, Ian Joughin, Matt A. King, Jan

T. M. Lenaerts, Jilu Li, Stefan R. M. Ligtenberg, Adrian Luckman, Scott B. Luthcke, Malcolm McMillan, Rakia Meister, Glenn Milne, Jeremie Mouginot, Alan Muir, Julien P. Nicolas, John Paden, Antony J. Payne, Hamish Pritchard, Eric Rignot, Helmut Rott, Louise Sandberg Sørensen, Ted A. Scambos, Bernd Scheuchl, Ernst J. O. Schrama, Ben Smith, Aud V. Sundal, Jan H. van Angelen, Willem J. van de Berg, Michiel R. van den Broeke, David G. Vaughan, Isabella Velicogna, John Wahr, Pippa L. Whitehouse, Duncan J. Wingham, Donghui Yi, Duncan Young, and H. Jay Zwally. A reconciled estimate of ice-sheet mass balance. *Science*, 338(6111):1183–1189, 11 2012. URL <http://www.sciencemag.org/content/338/6111/1183.abstract>.

Michael Sigl, Joseph R. McConnell, Lawrence Layman, Olivia Maselli, Ken McGwire, Daniel Pasteris, Dorte Dahl-Jensen, J. P. Steffensen, Bo Vinther, Ross Edwards, Robert Mulvaney, and Sepp Kipfstuhl. A new bipolar ice core record of volcanism from WAIS Divide and NEEM and implications for climate forcing of the last 2000 years. *Journal of Geophysical Research: Atmospheres*, 118(3):1151–1169, 2013. ISSN 2169-8996. doi: 10.1029/2012JD018603. URL <http://dx.doi.org/10.1029/2012JD018603>.

Mehrdad Soumek. *Synthetic Aperture Radar Signal Processing With Matlab Algorithms*. John Wiley & Sons Inc., New Jersey, United States, 1st edition, 1999.

Todd Sowers. Atmospheric methane isotope records covering the Holocene period. *Quaternary Science Reviews*, 29(1–2):213 – 221, 2010. ISSN 0277-3791.

doi: 10.1016/j.quascirev.2009.05.023. URL <http://www.sciencedirect.com/science/article/pii/S0277379109001899>.

Vandy B. Spikes, Gordon S. Hamilton, Steven A. Arcone, Susan Kaspari, and Paul A. Mayewski. Variability in accumulation rates from GPR profiling on the West Antarctic plateau. *Annals of Glaciology*, 39(1):238–244, June 2004. URL <http://www.ingentaconnect.com/content/igsoc/agl/2004/00000039/00000001/art00037>.

Vandy Blue Spikes, Beáta M. Csathó, and Ian M. Whillans. Laser profiling over Antarctic ice streams: methods and accuracy. *Journal of Glaciology*, 49(165):315–322, 2003. URL <http://www.ingentaconnect.com/content/igsoc/jog/2003/00000049/00000165/art00015>.

Leigh A. Stearns, Benjamin E. Smith, and Gordon S. Hamilton. Increased flow speed on a large East Antarctic outlet glacier caused by subglacial floods. *Nature Geosci*, 1(12):827–831, 12 2008. doi: 10.1038/ngeo356. URL <http://dx.doi.org/10.1038/ngeo356>.

Eric J. Steig, David P. Schneider, Scott D. Rutherford, Michael E. Mann, Josefino C. Comiso, and Drew T. Shindell. Warming of the Antarctic ice-sheet surface since the 1957 International Geophysical Year. *Nature*, 457(7228):459–462, 01 2009a. URL <http://dx.doi.org/10.1038/nature07669>.

Eric J. Steig, David P. Schneider, Scott D. Rutherford, Michael E. Mann, Josefino C. Comiso, and Drew T. Shindell. Corrigendum: Warming of the Antarctic ice-sheet

surface since the 1957 International Geophysical Year. *Nature*, 460(7256):766–766, 08 2009b. URL <http://dx.doi.org/10.1038/nature08286>.

KJ Tinto and RE Bell. Progressive unpinning of Thwaites Glacier from newly identified offshore ridge: Constraints from aerogravity. *Geophysical Research Letters*, 38(20), 2011. doi: 10.1029/2011GL049026.

M. van den Broeke, W. J. van de Berg, and E. van Meijgaard. Snowfall in coastal West Antarctica much greater than previously assumed. *Geophysical Research Letters*, 33(L02505), 2006. doi: 10.1029/2005GL025239. URL <http://dx.doi.org/10.1029/2005GL025239>.

David G. Vaughan, Jonathan L. Bamber, Mario Giovinetto, Jonathan Russell, and A. Paul R. Cooper. Reassessment of net surface mass balance in Antarctica. *Journal of Climate*, 12(4):933–947, April 1999. URL [http://weblinks2.epnet.com/citation.asp?tb=1&\\_ua=bo+B%5F+shn+1+db+aphjnh+bt+ID++%229LS%22+8F11&\\_ug=sid+1E273D7C%2D90B5%2D44B1%2D9C72%2D9EF8052F2993%40sessionmgr2+db+aph+cp+1+4D2E&\\_us=frn+1+hd+False+or+Date+fh+False+ss+S0+sm+ES+sl+%2D1+dstb+ES+ri+KAAACB1D00007528+508E&\\_uh=btn+N+6C9C&\\_uso=st%5B2+%2D+st%5B1+%2DVaughan+st%5B0+%2DJN++%22Journal++of++Climate%22+tg%5B2+%2D+tg%5B1+%2DAU+tg%5B0+%2D+db%5B0+%2Daph+hd+False+op%5B2+%2DAnd+op%5B1+%2DAnd+op%5B0+%2D+mdb%5B0+%2Dimh+9DBB&fn=1&rn=1](http://weblinks2.epnet.com/citation.asp?tb=1&_ua=bo+B%5F+shn+1+db+aphjnh+bt+ID++%229LS%22+8F11&_ug=sid+1E273D7C%2D90B5%2D44B1%2D9C72%2D9EF8052F2993%40sessionmgr2+db+aph+cp+1+4D2E&_us=frn+1+hd+False+or+Date+fh+False+ss+S0+sm+ES+sl+%2D1+dstb+ES+ri+KAAACB1D00007528+508E&_uh=btn+N+6C9C&_uso=st%5B2+%2D+st%5B1+%2DVaughan+st%5B0+%2DJN++%22Journal++of++Climate%22+tg%5B2+%2D+tg%5B1+%2DAU+tg%5B0+%2D+db%5B0+%2Daph+hd+False+op%5B2+%2DAnd+op%5B1+%2DAnd+op%5B0+%2D+mdb%5B0+%2Dimh+9DBB&fn=1&rn=1).

David G. Vaughan, Andrew M. Smith, Hugh F. J. Corr, Adrian Jenkins, Charles R. Bentley, Mark D. Stenoien, Stanley S. Jacobs, Thomas B. Kellogg, Eric J. Rignot,



and Baerbel K. Lucchitta. *The West Antarctic Ice Sheet: Behavior and Environment*, volume 77 of *Antarctic Research Series*, chapter A Review of Pine Island Glacier, West Antarctica: Hypothesis of Instability vs. Observations of Change, pages 237–256. American Geophysical Union, 2001.

Edwin D. Waddington, Thomas A. Neumann, Michelle R. Koutnik, Hans-Peter Marshall, and David L. Morse. Inference of accumulation-rate patterns from deep layers in glaciers and ice sheets. *Journal of Glaciology*, 53(183):694–712, 2007. doi: 10.3189/002214307784409351. URL <http://www.ingentaconnect.com/content/igsoc/jog/2007/00000053/00000183/art00019>.

P. Wessel and W. H. F. Smith. New, improved version of Generic Mapping Tools released. *EOS Transactions of the American Geophysical Union*, 79(47):579, 1998.

Duncan A. Young, Scott D. Kempf, Donald D. Blankenship, John W. Holt, and David L. Morse. New airborne laser altimetry over the Thwaites Glacier Catchment, West Antarctica. *Geochemistry, Geophysics, Geosystems*, 9(6):Q06006, 2008. doi: 10.1029/2007GC001935. URL <http://dx.doi.org/10.1029/2007GC001935>.

H. Jay Zwally and Mario B. Giovinetto. Annual sea level variability induced by changes in sea ice extent and accumulation on ice sheets: an assessment based on remotely sensed data. *Surveys in Geophysics*, 18:327–340. (doi:10.1023/A:1006504530582), 1997.

## Vita

Erick Leuro attended “ Nicolas Esguerra” High School, Bogotá, Colombia. In 1991 he entered “Universidad Distrital, Francisco José Caldas”, Bogotá, Colombia. From 1994 to 2001 he was employed as a GIS/cadastral technician at the Public Works office of the city of Bogotá. He received the degree of Bachelor of Science on Surveying Engineering in 1997. In June 2001, he entered the Graduate School at The University of Texas at Austin, where he received the degree of Master of Science in Geological Sciences in May 2004. In January, 2008 he joined ION-GXT, Houston, TX as a geophysicist.

Permanent address: 3030 Elmside Dr. No 198. Houston, TX

This dissertation was typeset with  $\text{\LaTeX}^\dagger$  by the author.

---

<sup>†</sup> $\text{\LaTeX}$  is a document preparation system developed by Leslie Lamport as a special version of Donald Knuth’s  $\text{\TeX}$  Program.